Research Square

Preprints are preliminary reports that have not undergone peer review.
They should not be considered conclusive, used to inform clinical practice,
or referenced by the media as validated information.

Integrated Thermodynamic–Mechanical Analysis of a Combined ORC– VCC Refrigeration System Using an Expander–Compressor Unit-Based Piston for Waste-Heat Utilization

Panuwat Doungpateep
King Mongkut's University of Technology North Bangkok
Teerapharp Amornsawaddirak
King Mongkut's University of Technology North Bangkok
Kittiwoot Sutthivirode
King Mongkut's University of Technology North Bangkok
Suparat Jamsawang
King Mongkut's University of Technology North Bangkok
Tongchana Thongtip
tongchana.t@fte.kmutnb.ac.th
King Mongkut's University of Technology North Bangkok

Research Article

Keywords: Combined ORC-VCC, Coupled expander–compressor, Heat-driven refrigeration, low-grade waste heat

Posted Date: November 13th, 2026

DOI: https://doi.org/10.21203/rs.3.rs-11222936/v1

License: This work is licensed under a Creative Commons Attribution 4.0 International License.
Read Full License

Additional Declarations: No competing interests reported.

Integrated Thermodynamic–Mechanical Analysis of a Combined ORC–VCC Refrigeration System Using an Expander–Compressor Unit-Based Piston for Waste-Heat Utilization

Panuwat Doungpateep, Teerapharp Amornsawaddirak Kittiwoot Sutthivirode, Suparat Jamsawang and Tongchana Thongtip*

Thermal and Fluid Laboratory (TFL), Department of Teacher Training in Mechanical Engineering,
King Mongkut's University of Technology North Bangkok,
1518 Phacharat 1 Rd., Bang Sue, Bangkok 10800, Thailand

***** *Corresponding author. E-mail addresses: tongchana.t@fte.kmutnb.ac.th*

Abstract

This study presents a theoretical analysis of a directly coupled Organic Rankine Cycle–vapor-compression cycle (ORC–VCC), which is an alternative thermally driven refrigeration system. This system combines an ORC with a VCC via a free-piston expander-compressor unit (ECU). The ECU directly transfers mechanical work to a piston compressor without an intermediate generator, motor, or shaft train. A coupled thermodynamic–mechanical model is developed to assess piston force balance, swept volume, working-fluid mass flow rate, compressor work, cooling capacity, heat input, and system coefficient of performance (COP). Seven refrigerants, R134a, R22, R32, R410A, R1233zd(E), R1336mzz(E) and R1234yf are compared over generator temperatures of 60 – 90 °C, condenser temperatures of 30 – 45 °C, and evaporator temperatures of −10 to 10 °C. The results show that increasing generator or condenser temperature reduces COP, whereas increasing evaporator temperature and useful preheating improves COP. Mechanical parameters primarily scale cooling capacity because cooling output and required input increase in broadly similar proportions; consequently, they have little influence on COP under the idealized assumptions. R22 and R32 provide the highest calculated performance in most cases, while low-global-warming-potential fluids offer environmental advantages but lower predicted capacity under the investigated conditions. The findings establish design relationships for matching thermodynamic states to free-piston geometry and identify heat recovery, fluid selection, and operating temperatures as the principal levers for improving system-level efficiency.

Keywords: Combined ORC-VCC; Coupled expander–compressor; Heat-driven refrigeration; low-grade waste heat

Abbreviations

Nomenclature	
AR	Area Ratio
COP	Coefficient of Performance
ECU	Expander–Compressor Unit
GWP	Global Warming Potential
HCFC	Hydrochlorofluorocarbon
HCFO	Hydrochlorofluoroolefin
HFC	Hydrofluorocarbon
HFO	Hydrofluoroolefin
ODP	Ozone Depletion Potential
ORC	Organic Rankine Cycle
TDR	Thermally Driven Refrigeration machine
VCC	Vapour-Compression Cycle
A	Area (m^2)
b	Viscous-friction coefficient($N \cdot s \cdot m^{-1}$)
F	Force (N)
h	Enthalpy (kJ/kg)
k	Vapour specific-heat ratio
L	Piston stroke (m)
m	Mass (kg)
$\dot{m}$	Mass flow rate (kg/s)
N	Operating frequency ($strokes \cdot s^{-1}$)
f	Stroke frequency (Hz)
P	Pressure (kPa)
$\dot{Q}$	Heat rate (kW)
T	Temperature (^oC)
v	Specific volume ($m^3 \cdot kg^{-1}$)
V	Volume (m^3)
W	Work (kJ)
$\dot{W}$	Work rate (kW)
x	Piston displacement (m)
$\dot{x}$	Piston velocity ($m \cdot s^{-1}$)
$\ddot{x}$	Piston acceleration ($m \cdot s^{-2}$)
Subscripts and superscripts	
$comp$	Compressor
con	Condenser
$evap$	Evaporator
exp	Expander
exp, in	Expander inlet
f	Saturated liquid
g	Saturated vapour
fg	Phase change from liquid to vapour
gen	Vapour generator
lim	Limiting value
$preheat$	Preheating
$pump$	Feed pump
s	Swept volume
v	Volumetric
Greek symbols	
η	Isentropic efficiency

ρ	Density
Δ	Difference

1. Introduction

1.1 Background and literature review

Waste heat from industrial processes, internal-combustion engines, power-generation systems, and other energy-conversion processes is commonly rejected to the environment. A substantial fraction occurs at low-to-medium temperatures (approximately 60–200 °C), where conventional power-generation technologies are often technically or economically unattractive. Recovering this resource for cooling can reduce electricity demand, improve overall energy utilization, and lower indirect greenhouse-gas emissions.

Conventional Heat-driven refrigeration machines are based on absorption or ejector refrigeration cycles. Absorption systems use working pairs such as lithium bromide–water or ammonia–water and contain few moving parts, but their performance at low source temperatures can be constrained by a relatively low COP, corrosion, crystallization, and demanding heat and mass transfer control [1,4]. Ejector refrigeration systems are less complicated than absorption systems and can be powered by waste heat or low-grade heat; however, their COP is relatively low and strongly depends on ejector geometry and operating conditions. Performance deteriorates when the system deviates from its design point [5 – 7].

A considerable amount of the thermal energy supplied to industrial processes, internal-combustion engines, and power-generation units is mostly released to the environment as waste heat. A considerable part of this waste heat must be exploited at low or moderate temperatures, where traditional steam Rankine cycles are inefficient or not worth implementing. Organic Rankine cycles (ORCs) address this limitation by employing organic working fluids with comparatively low boiling temperatures. It enables to produce relatively high pressure at relatively low boiling temperature, resulting in high potential to produce useful mechanical power. Hence, low-grade heat can convert to useful mechanical power. If an ORC is mechanically coupled to a vapor-compression refrigeration cycle (VCC), it has high potential to convert waste heat directly into useful refrigeration. This is well known as the combined ORC-VCC. Hence, it is categorized as a thermally driven refrigeration machine (TDR). Unlike absorption and ejector refrigeration systems which are the most widely used TDR, an ORC–VCC configuration provides the relatively high cooling efficiency and controllability of mechanical vapour compression while replacing most of its external electrical input with thermally generated mechanical work [7 – 10].

Aphornratana and Sriveerakul [11] presented one of the earliest thermodynamic analyses of the ORC-VCC. They theoretically investigated the ORC-VCC using R22 and R134a as the working fluids and demonstrated that refrigeration could be produced from thermal energy at temperatures as low as approximately 60 °C, while achieving evaporator temperatures down to −10 °C. Their work established the feasibility of heat-powered mechanical refrigeration and showed that system performance was strongly affected by generator, condenser, and evaporator temperatures. Nevertheless, their analysis treated the expander and compressor primarily through thermodynamic work balances and did not determine the piston dimensions required for direct reciprocating coupling.

Wang et al. [12] developed and tested a combined ORC–VCC system to recover waste heat from stationary and mobile engines. Their results showed that engine coolant and exhaust heat can be converted into useful cooling for buildings and vehicles. This work highlighted the potential to reduce electrically driven cooling loads when waste heat and refrigeration demand coincide. Wang et al. [13] further compared system configurations, demonstrating that component integration, fluid selection, and operating conditions significantly affect overall COP. They focused on rotating expanders, compressors, and conventional power transmission. The relationship between pressure forces and the geometry of a directly coupled reciprocating unit remains largely unexplored.

Recent advancements in solar-driven applications have expanded the potential of the organic Rankine cycle–vapor-compression cycle (ORC–VCC) concept [14 - 16]. Bu et al. [17] studied a solar-powered organic Rankine–vapour-compression ice-making system, evaluating how operating conditions and working-fluid selection affect performance. Their findings show that solar heat can supply both the thermal input for the ORC and the mechanical power for the refrigeration compressor. The analysis also highlights that optimal performance is associated with the thermodynamic properties of the ORC and VCC fluids and the heat-source and refrigerating temperatures. Li et al. [18] assessed hydrocarbon fluids for a Rankine-cycle-driven VCC using low-grade thermal energy. Although

hydrocarbons offer favorable thermodynamic performance due to suitable saturation characteristics and transport properties, their flammability is a significant limitation. Overall, these studies suggest that working-fluid selection should consider not only the coefficient of performance (COP) but also safety, operating pressure, environmental impact, and component compatibility.

Molés et al. [19] provided an important contribution by investigating low-global-warming-potential fluids in a combined ORC–VCC system activated by low-temperature heat. They compared different low-GWP fluid pairs over a range of operating conditions and reported system thermal COP values of approximately 0.30–1.10. Their results showed that ORC and VCC working-fluid selection must be implemented simultaneously because a fluid favorable for power generation does not always provide favorable refrigeration performance. The study also showed that generator, condenser, and evaporator temperatures substantially alter fluid rankings. This finding is particularly relevant to directly coupled systems because changes in saturation pressure affect not only thermodynamic performance but also the force available from the expander and the force required by the compressor.

Kim and Perez-Blanco [20] examined an integrated ORC–VCC system that generates both power and refrigeration. They discovered that distributing the ORC output between electricity generation and compressor operation increases operational flexibility, particularly under varying cooling demands. Nonetheless, initial electricity generation incurs losses in the generator, power electronics, and motor. For applications focused on refrigeration, a more straightforward conversion is achieved by directly transferring the expander work to the compressor; however, this necessitates a close match in speeds, torques, and operating ranges of both components. Saleh [21] evaluated a low-grade heat-driven ORC–VCC system, investigating the influence of heat-source temperature, evaporator and condenser temperatures, efficiencies of the expander and compressor, and the properties of working fluids on overall performance. The findings demonstrated that the system's coefficient of performance (COP) is highly dependent on the refrigeration temperature lift and the temperature differential within the ORC. Elevated evaporator temperatures enhance efficiency by reducing compressor work, whereas higher condenser temperatures diminish system performance. This effect is particularly pronounced in integrated systems, where increased condenser pressure elevates the compressor's pressure lift and reduces the expansion pressure differential.

Nasir and Kim [22] expanded fluid screening and optimization for ORC–VCC air-conditioning systems driven by low-grade heat. They compared single- and dual-fluid arrangements, showing that independently selecting the ORC working fluid and VCC refrigerant improves performance by allowing each cycle to operate with a fluid suited to its temperature and pressure range. Their study highlighted critical temperature, saturation pressure, latent heat, vapor density, and environmental characteristics as major fluid-selection criteria. However, dual-fluid arrangements require separate heat-rejection circuits or an extra heat exchanger, increasing system complexity. Single-fluid systems can be more compact but must meet both power production and refrigeration needs. While earlier work focused on thermodynamics, Marion and Louahlia [23] addressed the volumetric design of ORC–VCC compressor–expander units. They showed that displacement matching is vital because ORC and VCC often need different flow rates. The needed swept-volume ratio depends on fluid density, pressure ratio, efficiency, and temperature. This research advanced toward practical hardware by linking cycle calculations to machine dimensions. However, volumetric compatibility alone doesn't ensure stable operation; a directly coupled reciprocating system must also satisfy force balance, and piston areas must convert pressure differences into sufficient compression force.

Grauberger et al. [24] conducted a key experimental demonstration of ORC-driven vapour-compression cooling. They built a 300-kW-class system using the low-GWP refrigerant R1234ze(E), with the ORC turbine and refrigeration compressor on a common shaft. At a waste-heat-stream temperature of about 91 °C, a heat-rejection temperature of 30 °C, and a chilled-water temperature of 7 °C, the system produced (264 \pm 3.5) kW of cooling and achieved an overall COP of (0.56 \pm 0.01). The measured isentropic efficiencies were approximately 76.7% for the turbine and 84.8% for the compressor. The study also found that heat-exchanger and piping pressure drops were higher than predicted, reducing performance. These results confirm the technical feasibility of ORC–VCC cooling at scale and highlight the need to account for real component losses rather than relying only on ideal cycle calculations.

Sleiti et al. [25] experimentally studied a thermo-mechanical refrigeration system powered by ultra-low-temperature waste heat between about 50 and 85 °C. This range is directly relevant to industrial cooling water, engine coolant, and low-temperature process streams. The experiments confirmed that ORC-driven refrigeration can operate

under these conditions, but also revealed strong sensitivity to heat-source temperature, condenser and evaporator conditions, working fluid, and component selection. This is significant because low-grade waste-heat sources often fluctuate in practice. As a result, systems designed only for nominal conditions may experience significant drops in cooling output or stability under off-design scenarios.

More recently, Alshammari et al. [26] studied a single-rotor expander–compressor device for a combined ORC–VCC system. Their validated numerical model included ORC evaporation temperatures of about 62.75–89.7 °C, VCC evaporation temperatures of −20 to 5 °C, condenser temperatures of 20–45 °C, and rotor speeds from 500 to 3000 rpm. Under optimal conditions, the maximum cooling output, heat-to-cooling efficiency, and exergy efficiency were 5.38 kW, 56%, and 63%, respectively. Cooling capacity increased nearly linearly with rotational speed, while heat-to-cooling and exergy efficiencies remained largely unchanged. This suggests that geometric displacement and operating frequency mainly determine system capacity, while thermodynamic state points and fluid properties govern efficiency. Recent optimization and review studies have confirmed these results.

Witanowski [27] showed that optimizing the choice of working fluid and operating conditions is necessary to balance cooling output, power generation, and waste-heat use. Suchocki [28], in his comprehensive review of ORC–VCC technology, stated that selection of the working fluid, component efficiency, thermal integration, and the matching of the expander and compressor are areas which remain priorities for ongoing research. The review also noted that experimental studies are far less common than steady-state thermodynamic simulations, particularly for compact, mechanically integrated devices.

Overall, the published literature demonstrates that ORC–VCC systems can convert low-grade waste or solar heat into useful refrigeration, and their performance is strongly governed by heat-source temperature, condenser and evaporator conditions, component efficiencies, and working-fluid properties. Experimental investigations have established technical feasibility, while working-fluid screening and optimization studies have identified promising operating regions. However, most existing work treats the expander and compressor as independent components connected by a rotating shaft, an electrical link, or an ideal work balance. By comparison, relatively little attention has been given to a free-piston expander–compressor in which the ORC and VCC are coupled through both piston displacement and instantaneous pressure forces.

1.2 Research gap and contribution

Most published ORC–VCC research emphasizes thermodynamic models, exergy analysis, or working fluid screening. Few explicitly couple these quantities to the force balance and displacement of a reciprocating expander–compressor. This omission limits the ability to translate cycle-level results into realizable piston areas, strokes, frequencies, mass flow rates, and cooling capacities.

Three additional gaps motivate the present work. First, many studies compare only a small subset of fluids or a single refrigerant family, limiting cross-family interpretation. Second, the effect of recovering expander-exhaust heat to preheat the liquid entering the generator has not been assessed systematically for the proposed mechanism. Third, the quantitative links among piston geometry, mass-flow production, cooling capacity, and COP remain insufficiently reported for a directly coupled free-piston system.

This study bridges the gap by integrating thermodynamic state equations with the mechanical design of a directly coupled free-piston system. It introduces the compressor-to-expander piston-area ratio as a key mechanical matching parameter, determined by the pressures in the generator, condenser, and evaporator. Additionally, it links piston cross-sectional area, stroke length, and operating frequency to refrigerant mass flow rate, cooling capacity, compressor work, and heat input to the generator. Seven refrigerants, R134a, R1233zd(E), R1336mzz(E), R22, R32, R410A, and R1234yf, are evaluated under specified operating conditions, with an internal heat recovery of expander-exhaust heat through liquid preheating. This integrated thermodynamic–mechanical approach yields insights beyond cycle performance alone and provides an initial framework for transforming low-grade-heat-driven refrigeration from a conceptual cycle into a physically matched reciprocating machine.

The specific objectives are to: quantify cooling capacity, mass flow rate, work, heat input, and COP for source temperatures of approximately 60–90 °C; compare R134a, R1233zd(E), R22, R32, R410A, and R1234yf; and establish how piston area, stroke, and operating frequency affect capacity and performance.

2. System description and mathematical model

2.1 System configuration and operating principle

The proposed system is a heat-driven refrigeration machine that directly couples an organic Rankine cycle (ORC) with a vapor-compression refrigeration cycle (VCC) via a free-piston expander–compressor unit (ECU). Fig. 1 shows the schematic view of the proposed system. Low-grade waste heat supplies thermal energy to the ORC side, and the mechanical work produced during expansion is transferred directly to the VCC compressor. This design eliminates the need to convert mechanical power to electricity and removes the electrical drive required for a conventional compressor. It reduces energy-conversion losses, uses fewer components, and simplifies the system, while the refrigerating purpose can be directly powered by a relatively low heat source.

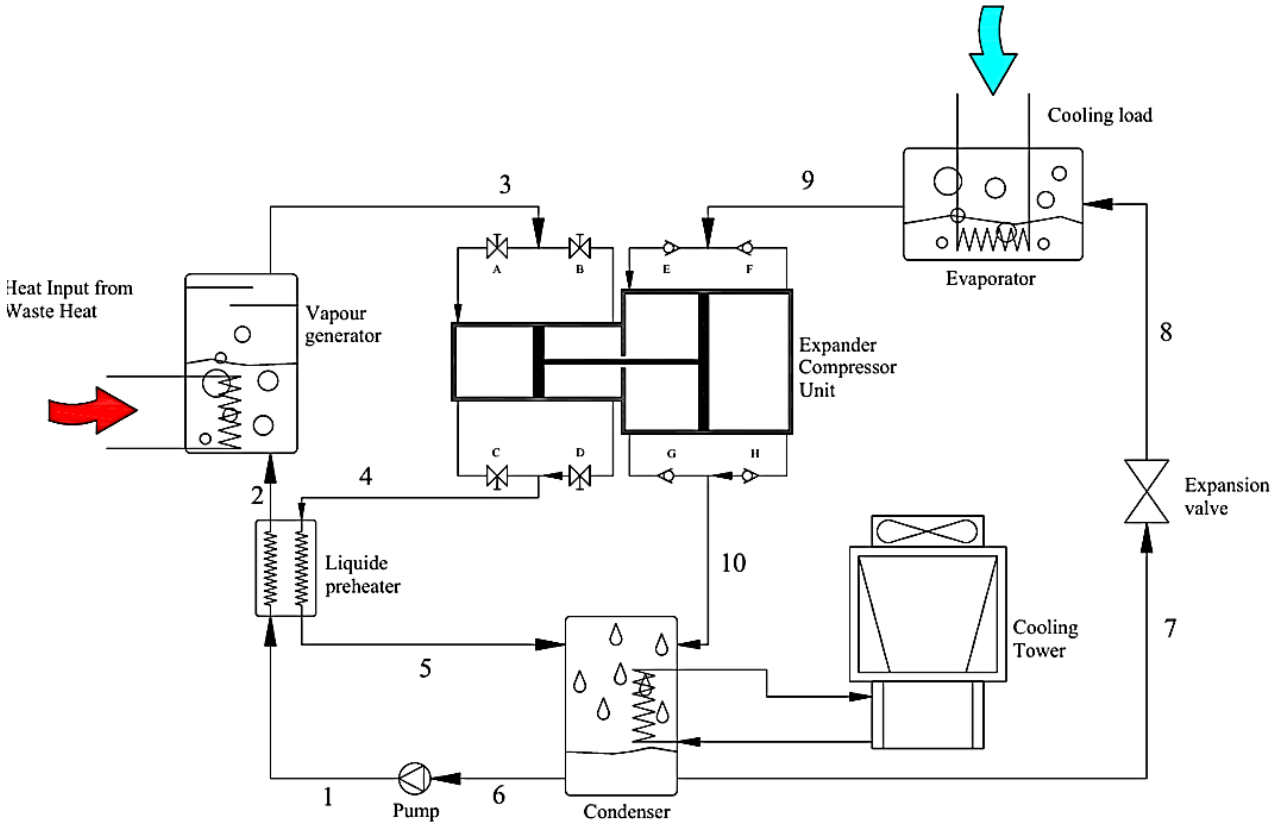


Fig. 1: Schematic of the combined ORC-VCC with a directly coupled expander–compressor.

On the ORC side, the liquefied refrigerant is pressurized by the feed pump and passes through a liquid preheater before entering the vapor generator. The preheater recovers sensible heat from the hot expander exhaust, increasing the liquid's inlet temperature and reducing the heat rate in the vapor generator. The liquid refrigerant is then vaporized to produce high-pressure but low-temperature vapor. This high-pressure vapor is supplied alternately to the two chambers of the double-acting expander (ECU) as shown in Fig. 2, where its pressure

energy converts into reciprocating piston work. After expansion, the working fluid is discharged to the condenser and returned to the pump, completing the ORC cycle.

The ECU assembly constitutes the primary thermodynamic and mechanical connection between the two cycles. The ORC expander piston is directly connected to a VCC compressor piston, ensuring both pistons operate with the same stroke and frequency. The piston cross-sectional area of the ECU may be different, allowing the ORC-supplied pressure forces to match the VCC's requirements. Consequently, the expander-to-compressor area ratio is a fundamental design parameter, not merely a geometric choice. This is because it determines whether the pressure differential across the expander can generate enough force to compress the refrigerant from evaporator pressure to condenser pressure. Section 2.2 will detail this.

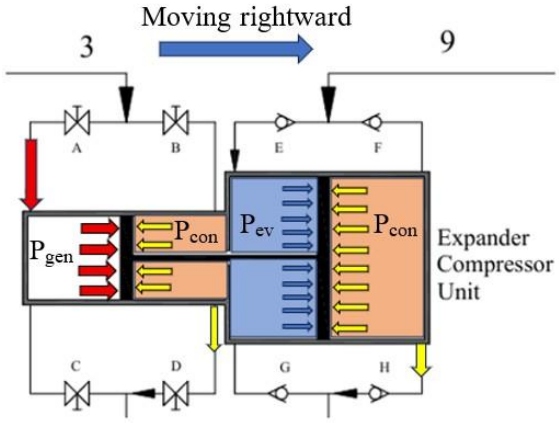


Fig. 2: The pressure force diagram of the ECU

To operate the ECU, the coordinated valve operation facilitates reciprocating motion. Referring to Fig. 2, on the expander side, valves A and B alternately experience high-pressure vapor from the generator, whereas valves C and D discharge expanded fluid from the opposite chamber to the condenser. During the rightward stroke, valves A and D are open, and valves B and C are closed. High-pressure vapor enters through valve A and exerts force on the left face of the expander piston, thereby moving the assembly to the right as fluid in the right chamber is expelled through valve D. For the return stroke, valves A and D are closed, while valves B and C are open, reversing the roles of expansion and discharge. This alternating sequence ensures that both sides of the expander sustain continuous reciprocating motion.

On the VCC side, check valves E–H automatically regulate refrigerant suction and discharge based on instantaneous chamber pressures. During rightward piston motion, refrigerant vapor in the right compressor chamber is compressed. When its pressure exceeds the condenser pressure, discharge valve H opens, allowing the compressed vapor to flow to the condenser. At the same time, the increasing volume of the left compressor chamber lowers its pressure. This causes suction valve E to open and draw low-pressure vapor from the evaporator. During leftward motion, the functions reverse: the left chamber compresses and discharges, while the right chamber draws in suction. The double-acting configuration produces a compression process during each piston stroke and supports quasi-continuous refrigerant circulation.

After leaving the compressor, the high-pressure refrigerant releases heat to the surroundings. It then condenses in the condenser as cooling water is supplied. The liquefied refrigerant then expands through the expansion device. Its pressure and temperature decrease before it enters the evaporator. At the evaporator, the cooling load is absorbed during evaporation, producing the refrigeration effect, and the resulting low-pressure vapor returns to the compressor to complete the cycle. Cooling capacity depends on the compressor's swept volume, piston frequency, refrigerant suction density, and the enthalpy change at the evaporator. A key aspect of the proposed system is the heat recovery of the expander exhaust. Because this stream may remain hotter than the pressurized liquid leaving the pump, the liquid preheater can recover residual thermal energy. This internal

heat recovery reduces external generator heat duty without directly affecting the cooling load, thereby improving the overall thermal coefficient of performance (COP).

Overall, the proposed system integrates thermal-energy recovery, direct mechanical power transmission, and vapor-compression refrigeration in a compact architecture. Its main advantage is to directly convert low-grade waste heat into the refrigeration cycle without an electrical conversion stage. However, successful operation depends on matching ORC and VCC pressure levels to the piston cross-sectional areas, coordinating expander valve timing, and maintaining stable piston motion under varying heat-source, condenser, and evaporator conditions. These coupled requirements distinguish the proposed system from conventional shaft-driven ORC–VCC arrangements and make the free-piston geometry and control strategy central to its practical feasibility. This work discusses these aspects.

2.2 Governing equations

2.2.1 Force balance at the ECU

According to the ECU, the expander and compressor can be operated via pressure force exerting on the piston and work balances between them. The two pistons move together, and their cross-sectional areas is different. By neglecting friction, leakage, piston inertia, and mechanical transmission losses, the minimum or limiting area ratio between the two pistons can be determined by the pressure forces acting on the two sides of the ECU as previously shown in Fig. 2.

$$AR_{lim} = \frac{A_{com}}{A_{exp}} = \frac{P_{gen} - P_{con}}{P_{con} - P_{evap}} \tag{1}$$

where A denotes piston cross-sectional area, and P denotes the applicable chamber pressure. The resulting relation provides the geometric match required for quasi-static force balance at the specified generator, condenser, and evaporator pressures.

For the practical operation of the free-piston expander-compressor unit, it is governed by the instantaneous force balance acting on the mechanically connected piston assembly. Taking piston motion toward the right as positive, the governing equation can be expressed as,

$$\mathrm{m_p}\frac{\mathrm{d^2x}}{\mathrm{dt^2}} = A_{exp}\left(P_{gen} - P_{con}\right) + A_{com}\left(P_{con} - P_{evap}\right) - F_f \tag{2}$$

where m_p is the total moving mass, x is the piston displacement, P_{gen}, P_{con} and P_{evap} are the generator pressure, the condenser pressure and the evaporator pressure, respectively. F_f is the friction force. Equation 2 represents the friction force.

$$\mathrm{Ff} = \mathrm{FC}\tanh(\dot{x}/v_0) + \mathrm{b}\,\dot{x} \tag{3}$$

where FC is the Coulomb-friction coefficient [29], b is the viscous-friction coefficient, and v_o is a small smoothing velocity.

During the rightward stroke, high-pressure vapor from the generator expands into the left expander chamber, while the right chamber connects to the condenser. Simultaneously, the refrigerant in the right compressor chamber is compressed toward the condenser pressure, while the left compressor chamber draws vapor from the evaporator. Under the idealized assumption of fully opened valves, the net driving force becomes

$$F_{net} = A_{exp}(P_{gen} - P_{con}) - A_{com}(P_{con} - P_{evap}) - F_f \quad (4)$$

The first term represents the force produced by the expander, whereas the second term is the opposing compressor force. During the leftward stroke, the chamber functions are reversed, but the force-balance relationship is theoretically identical because the ECU is double-acting.

For sustained operation, the selected area ratio must be smaller than this limiting value because part of the expander force is required to overcome friction and accelerate the piston:

$$\mathrm{AR} \leq \frac{\left[(P_{gen} - P_{con}) - \frac{\mathrm{Ff} + \mathrm{m_p}\ddot{\mathrm{x}}}{A_{exp}}\right]}{P_{con} - P_{evap}} \quad (5)$$

This relationship explains the trends observed in the area-ratio analysis. Increasing the generator temperature raises the generator saturation pressure, thereby increasing the available expander pressure difference. Consequently, a larger compressor piston can be driven, and the allowable area ratio increases. Conversely, increasing the common condenser temperature has two adverse effects. It increases the expander exhaust pressure, reducing the ORC driving-pressure differential, and it also raises the compressor discharge pressure, which in turn increases the refrigeration compression load. Consequently, the allowable area ratio decreases sharply with condenser temperature. Increasing the evaporator temperature reduces the compressor pressure ratio and opposing force; therefore, a larger compressor-to-expander area ratio is possible. This will be discussed in section 3.

2.2.2 Compression work required at the compressor side

The compression process at the compressor consists of an isentropic closed-system stage (1–2) and a constant-pressure discharge stage (2–3), which is represented by Fig. 3. During stage 1–2, saturated or specified suction vapor at $P_1 = P_{evap}$ is compressed to $P_2 = P_{con}$ before discharge begins. The isentropic compression work is derived from the first law for a closed system, together with the ideal-gas isentropic relation used in the source model:

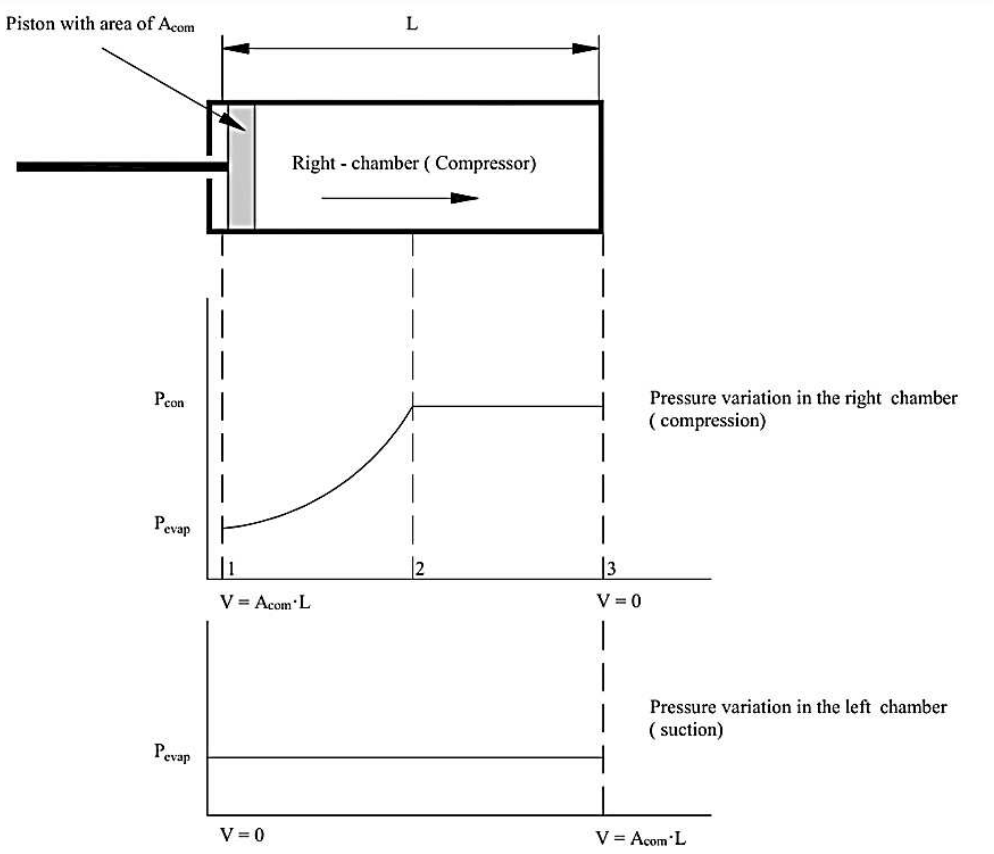


Fig. 3: The compression process at the compressor

$$P_1 \cdot {V_1}^k = P_2 \cdot {V_2}^k \tag{6}$$

$$w_{1\to2} = \frac{P_2 \cdot V_2 - P_1 \cdot V_1}{1-k} \tag{7}$$

After the pressure reaches the condenser pressure (P_{con}), the piston continues to move and releases refrigerant to the condenser at approximately constant pressure. The discharge work is then calculated as:

$$w_{2\to3} = P_2(V_3 - V_2) \tag{8}$$

$$w_{2\to3} = -P_2 \cdot V_2 \tag{9}$$

$$w_{com} = -\frac{V_1}{1-k} \cdot \left[k \cdot P_2 \left(\frac{P_1}{P_2}\right)^{\frac{1}{k}} - P_1 \right] \tag{10}$$

The clearance volume is assumed to be zero; therefore, no refrigerant remains in the compressor chamber at the end of discharge ($V_3 = 0$). The total compression-side work is the sum of the isentropic compression and constant-pressure displacement contributions:

$$W_{1\to3} = W_{1\to2} + W_{2\to3} \tag{11}$$

For each stroke, the suction volume equals the corresponding swept volume. The suction work is determined at evaporator pressure, and the double-acting symmetry gives the compressor work per complete reciprocating event. The refrigerant mass flow rate is obtained from swept volume, suction specific volume, and operating frequency.

$$W_{com-suction} = P_{evap} \cdot A_{com} \cdot L \tag{12}$$

$$W_{com-compression} = W_{com-suction} \tag{13}$$

$$\dot{W}_{com} = \frac{N \cdot A_{com} \cdot L}{1-k} \cdot \left[k \cdot P_{con} \left(\frac{P_{evap}}{P_{con}} \right)^{\frac{1}{k}} - P_{evap} \right] \tag{14}$$

The evaporator's cooling capacity is calculated from the refrigerant mass flow rate and the enthalpy change across the evaporator. This quantity represents the heat removed from the refrigerated space. The mass flow rate can be calculated using equation 15 while the cooling capacity can be calculated using equation 16.

$$\dot{m}_{evap} = \frac{N \cdot A_{com} \cdot L}{v_{g@T_{evap}}} \tag{15}$$

$$\dot{Q}_{evap} = \dot{m}_{evap} \cdot \left(h_{g@T_{evap}} - h_{f@T_{con}} \right) \tag{16}$$

On the ORC side, the generator vapor produced at P_{gen} expands to produce the mechanical work required by the compressor while also filling the expander swept volume. The corresponding working-fluid flow rate accounts for both displacement and work done. Because compressor work is a major requirement from the ORC side, this means the work done by the ORC's expander is equal to the work required for the VCC's compressor. The external heat supplied to the generator is evaluated from the working-fluid mass flow rate and the enthalpy increase between the generator inlet and outlet as stated in equations 17 and 18.

$$\dot{m}_{gen} = \frac{N \cdot A_{exp} \cdot L}{v_{g@T_{gen}}} + \frac{|\dot{W}_{com}|}{h_{fg@T_{gen}}} \tag{17}$$

$$\dot{Q}_{gen} = \dot{m}_{gen} \cdot \left(h_{g@T_{gen}} - h_2 \right) \tag{18}$$

For the preheated cases, the liquid temperature upstream of the generator is specified as T2 = Tcon + $\Delta T_{preheat}$. In this work, the preheating temperature is fixed throughout at 15 °C. The recovered heat is assumed to originate from the hot expander exhaust. Without preheating, the inlet liquid temperature equals the condensation temperature.

Pump power is calculated by treating the working fluid as incompressible and the pumping process as an isentropic process. It depends on mass flow rate, saturated-liquid specific volume, and the pressure rise from the condenser to the generator, which can be determined by equation 19:

$$\dot{W}_{pump} = \dot{m}_{gen} \cdot v_{f@T_{con}} \left(P_{gen} - P_{con} \right) \tag{19}$$

The overall system coefficient of performance is defined as the evaporator cooling rate divided by the sum of external generator heat input and pump power:

$$COP_{combined} = \frac{\dot{Q}_{evap}}{\dot{Q}_{gen} + \dot{W}_{pump}} \tag{20}$$

Because this analysis neglects component irreversibilities and several mechanical losses, the calculated COP represents an idealized upper-bound performance under the stated conditions.

2.3 Working-fluid candidates

The working-fluid selection is significant for the proposed combined ORC–VCC system. This is because the same fluid must satisfy two distinct thermodynamic requirements. On the ORC side, the fluid should deliver adequate saturation pressure and expansion work at the available waste-heat temperature. This must avoid approaching the critical point too closely. On the refrigeration side, it must provide sufficient suction-vapor density, refrigeration effect, and a reasonable compressor pressure ratio. Because the expander and compressor are directly coupled, fluid selection also influences instantaneous piston-force equilibrium, the required piston-area ratio, operating frequency, and achievable cooling capacity. Consequently, fluids cannot be evaluated solely based on COP or ORC efficiency.

Seven working fluid candidates were considered for this work including R22, R134a, R32, R410A, R1234yf, R1233zd(E), and R1336mzz(E). Table 1 summarizes the physical properties of these working fluids. Thermophysical properties are based on saturation-property data, and refrigerant designations and chemical identities follow ASHRAE nomenclature. ASHRAE refrigerant designations distinguish pure fluids from R410A, which is a near-azeotropic blend of R32 and R125.

Table 1: The properties of the working fluids

Fluid	Chemical family or composition	Molar mass (g mol^{-1})	Normal boiling point (°C)	Critical temperature (°C)	Critical pressure (MPa)	Safety class	ODP	Indicative GWP_{100}
R22	HCFC; $CHClF_2$	86.47	−40.81	96.15	4.990	A1	0.055	1,810
R134a	HFC; CF_3CH_2F	102.03	−26.07	101.06	4.059	A1	0	1,430
R32	HFC; CH_2F_2	52.02	−51.65	78.11	5.783	A2L	0	675
R410A	R32/R125, 50/50 mass%	72.59	−51.44	71.34	4.901	A1	0	2,088
R1234yf	HFO; $CF_3CF=CH_2$	114.04	−29.46	94.70	3.384	A2L	0	<1†
R1233zd(E)	HCFO; trans-$CF_3CH=CHCl$	130.50	18.13	165.71	3.583	A1	≈0.0003	≈1
R1336mzz(E)	HFO; trans-$CF_3CH=CHCF_3$	164.05	7.87	130.38	2.779	A1	0	≈18

R22 and R134a serve as reference cases due to their well-known thermodynamic and heat-transfer properties. Both are A1, indicating lower toxicity and non-flammability. R22 has high vapor pressure and capacity but is unsuitable for new long-term use because of ozone depletion and HCFC status. R134a has zero ODP and moderate pressure, but high GWP reduces its environmental appeal. They are best kept as benchmarks rather than recommended for practical use.

R32 and R410A exhibit high vapor pressures and densities under refrigeration conditions, resulting in high volumetric cooling capacity and significant cooling output. Their high pressures also generate substantial compressor force for a given piston area. However, their low critical temperatures limit their suitability for ORC applications. At a generator temperature of 70 °C, R410A operates near its pseudo-critical temperature of 71.3 °C, and R32 has a critical temperature of 78.1 °C. In this range, saturation properties change rapidly, latent heat decreases, and small temperature shifts can significantly affect density, pressure, and expander performance. As a blend, R410A may also cause composition shifts and temperature glide. Therefore, R32 and especially R410A are less suitable for strictly subcritical ORC operation near 70 °C. Generator temperatures should remain below their critical limits unless a transcritical model and suitable property database are used.

R1233zd(E) and R1336mzz(E) offer higher critical temperatures, making them suitable for low- and medium-temperature waste-heat recovery. Their broad subcritical temperature ranges minimize generator pressure sensitivity to temperature fluctuations and allow greater control over vapor superheat. Both fluids are classified as A1 and have very low environmental impact. R1336mzz(E), for instance, is nonflammable, has low GWP, and is suitable for high-temperature heat pumps and ORCs, with a critical temperature near 130.4 °C. However, both fluids have relatively high normal boiling points. At an evaporator temperature of 10 °C,

R1233zd(E) operates below atmospheric pressure, while R1336mzz(E) operates only slightly above it. As a result, their compressor-suction vapor densities are low, leading to reduced refrigerant mass flow rates and cooling capacities for a given compressor displacement. Sub-atmospheric operation also increases the risk of air and moisture ingress. Therefore, while these fluids are promising for ORC applications, they are less suitable when a single fluid and compact compressor must serve both cycles.

R1234yf offers a balanced compromise. Its saturation-pressure range is similar to R134a, and its critical temperature of about 94.7 °C provides a sufficient subcritical margin above the generator temperature of 70 °C. With zero ODP and very low GWP, R1234yf is environmentally preferable to R134a, R22, and R410A. Its main drawback is its A2L classification, which means low toxicity but mild flammability. Therefore, minimizing refrigerant charge, ensuring ventilation, implementing leak detection, removing ignition sources, and complying with safety standards are essential for both experimental and practical use.

2.4 Computational Procedure for the Combined ORC–VCC Model

The thermodynamic performance of the mechanically coupled ORC–VCC system was evaluated using a numerical model developed in MATLAB. Numerical implementation is necessary because the system contains strongly coupled, nonlinear relationships among working-fluid properties, operating temperatures, mass flow rates, component efficiencies, and the geometry of the free-piston expander–compressor unit (ECU). The model simultaneously determines the thermodynamic properties, the energy and exergy flows, and the expander-to-compressor mechanical balance. This framework enables systematic comparison of candidate fluids and operating conditions while maintaining a consistent set of component assumptions.

MATLAB was used as the principal computational environment because it can perform iterative numerical solutions, structured data handling, sensitivity analysis, and automated post-processing. The program solves the steady-state mass and energy balances. Iteration is required when a state variable depends implicitly on pressure, temperature, phase condition, or mechanical coupling. The same solver was embedded in nested parameter loops to vary the generator temperature (T_{gen}), condenser temperature (T_{con}), evaporator temperature (T_{evap}), piston stroke, and operating frequency. The resulting data were used to quantify generator heat input, cooling capacity, coefficient of performance (COP), mass flow rate, and the required piston-area ratio. An advantage of this implementation is that the thermodynamic and geometric calculations are performed within a single solution sequence. Consequently, a nominally favorable cycle condition is accepted only when it also satisfies the ECU force requirement and the prescribed operating limits. This coupling is important because the expander doesn't produce electricity; instead, its pressure work is directly transferred to the compressor piston.

Thermophysical properties were obtained from the open-source CoolProp library (Bell et al., [30]), accessed via its Python interface from MATLAB. This methodology avoids interpolation errors associated with tabulated data and provides a consistent property-computation routine for all candidate working fluids. Enthalpy, entropy, density, specific volume, vapor quality, saturation pressure, and critical properties were derived from two independent state variables. Cases at or above the critical boundary were omitted from the current subcritical model. This restriction is particularly pertinent to R32 and R410A, as the investigated generator-temperature range approaches the critical region. The procedure ensures that saturation-based formulations are not extrapolated into domains where they are undefined.

The iterative loops were terminated when the maximum normalized change in the calculated variables between two successive iterations was below 10^{-6}. In addition, the residuals of the energy balances and the mechanical coupling equation were monitored. A case was rejected if the property routine failed, the specified state exceeded the adopted subcritical domain, a non-positive density or mass flow rate was obtained, or the calculated phase condition was incompatible with the component.

After convergence, the program exported the state-point data and performance indicators to a structured spreadsheet for plotting and statistical comparison. The automated framework permits rapid screening of refrigerants

and operating parameters, identification of system performance, and evaluation of the recuperative preheater before prototype manufacture. It also demonstrates the trade-off between thermodynamic performance and ECU size. This means that system COP depends significantly on an area ratio, pressure load, or piston displacement. Accordingly, the model is best interpreted as a design-screening and operating-envelope tool.

3. Results and Discussion

3.1 Force balance and significance of the expander-compressor piston-area ratio

The practical operation of the free-piston expander-compressor unit is governed by the instantaneous force balance acting on the mechanically connected piston assembly. Section 2.2 previously presented the force-balance equation. According to the ECU, the expander and compressor can be operated via the pressure force on the piston and the work balance between them. The two pistons move together, but their cross-sectional areas differ. In this case, the compressor piston cross-sectional area is fixed at 25 $cm^{2,}$ and the stroke is fixed at 20 cm throughout the discussion. This means the AR's ECU varies with the expander piston size. This section discusses the ECU's limited piston area ratio under various working conditions and working fluids.

3.1.1 The limiting area ratio (A_{com}/A_{exp}) against the working temperature of the generator, evaporator and condenser

Fig. 4 shows the limiting area ratio of the ECU as a function of generator temperature under fixed condenser and evaporator operating conditions. It shows that increasing the generator temperature from 60 to 90 °C increases the required area ratio for all investigated working fluids. The increase is nonlinear and becomes more pronounced at higher generator temperatures. The AR increases from approximately 0.5 – 0.65 at 60 °C to about 2.0 – 2.6 at 90 °C, depending on the working fluid.

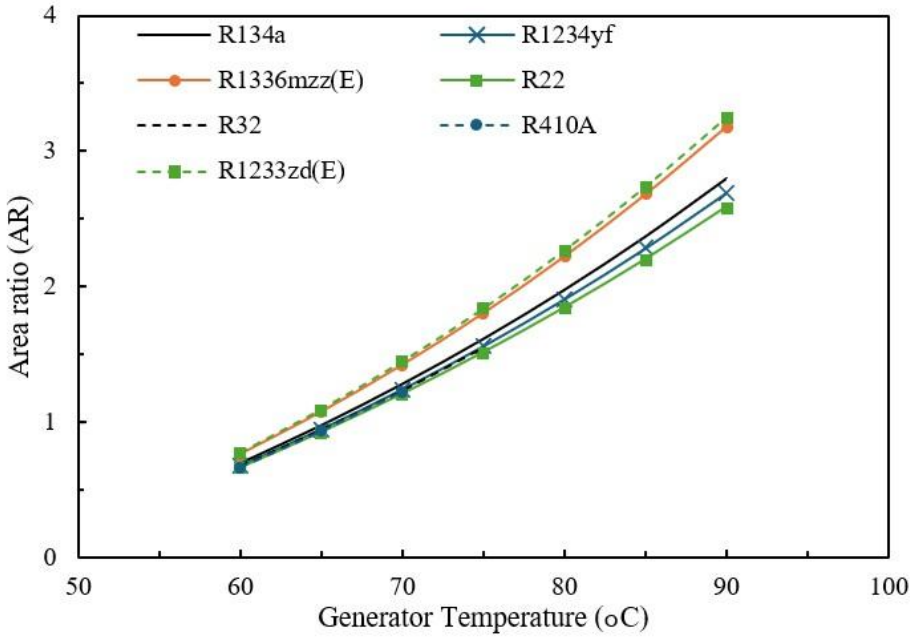


Fig. 4: The ECU's area ratio against the generator temperature

This behavior is primarily caused by increased generator saturation pressure. Because the condenser and evaporator temperatures are maintained at 45 and −10 °C, respectively. The compressor-side pressure difference remains approximately constant. In contrast, the pressure difference across the expander increases as the generator

temperature rises. A greater expansion force is produced for a given expander-piston area. Under the condition of a fixed compressor area, the force balance can be satisfied using a smaller expander area, leading to an increase in $A_{\mathrm{com}}/A_{\mathrm{exp}}$.

The increasing slope at high generator temperatures has an important practical implication. The mechanical matching condition becomes progressively more sensitive to heat-source temperature at relatively high generator temperature. A piston assembly designed at 60 – 70 °C may therefore become substantially over-driven when exposed to a 90 °C heat source. The resulting excess expansion force could produce excessive piston acceleration, elevated impact loads near the stroke limits, unstable valve timing, and increased mechanical losses. Conversely, selecting the area ratio at the highest generator temperature may result in insufficient expansion force when the waste-heat temperature decreases. This means the ECU must carefully consider the AR for a specified operating condition.

Differences among the fluids are mainly because of their saturation-pressure characteristics. R1233zd(E) and R1336mzz(E) generally require the largest AR values, while R22 gives lower ratios at the upper end of the temperature range. However, a high AR should not be interpreted as evidence of superior thermodynamic performance. It indicates that the pressure differences generated by a particular fluid require a different piston geometry to achieve mechanical equilibrium. This means working-fluid selection must consider COP and cooling capacity alongside the corresponding cylinder dimensions and operating-pressure levels.

The condenser temperature produces the strongest and most mechanically unfavorable influence among the three investigated temperatures. As shown in Fig. 5, increasing $T_{\mathrm{con}}$from 30 to 45 °C reduces AR from approximately 1.5 – 1.9 to only about 0.50 – 0.65. This sharp decline occurs because condenser pressure affects both sides of the coupled unit simultaneously. On the ORC side, increasing P_{con}reduces the available expander pressure difference. At the same time, it increases the pressure difference the refrigeration compressor must overcome; thus, the driving force decreases while the resisting force increases. To maintain mechanical balance when the compressor piston's cross-sectional area is fixed, the expander piston area must increase substantially, reducing AR.

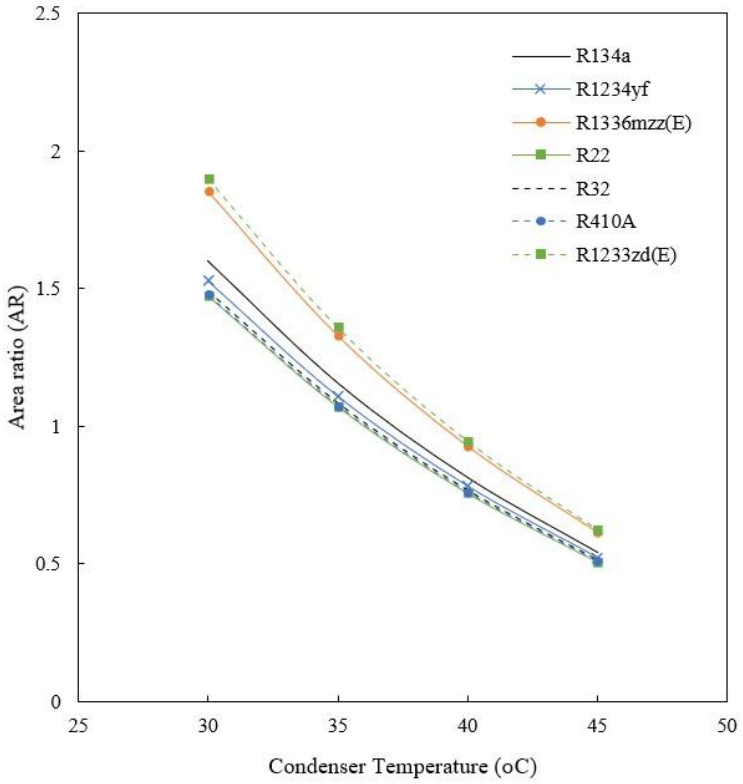


Fig. 5: The ECU's area ratio against the condenser temperature

The convergence of fluid curves at higher condenser temperatures is significant. At 30 °C, the required ratios vary considerably among fluids, but at 45 °C, they fall within a much narrower range. Under severe heat-rejection conditions, condenser pressure becomes a dominant factor, reducing the impact of individual fluid properties. Therefore, enhancing condenser heat transfer may provide greater practical benefits than choosing a fluid based only on its nominal thermodynamic performance.This finding is especially important for systems in hot climates or those with air-cooled condensers. Higher ambient temperatures can reduce COP, increase generator heat demand, and disrupt optimal piston geometry. The condenser should be sized for the maximum expected heat-sink temperature, not the annual mean. Sufficient heat-transfer area, controlled airflow, low fouling resistance, and a minimal refrigerant-to-ambient temperature difference are essential to maintain thermodynamic performance and stable piston motion.

Fig. 6 demonstrates that AR increases moderately as the evaporator temperature rises from −10 to 10 °C. The required ratios increase from approximately 0.50–0.60 to about 0.65–0.75, depending on the working fluid. This effect is less significant than the influence of generator and condenser temperatures.

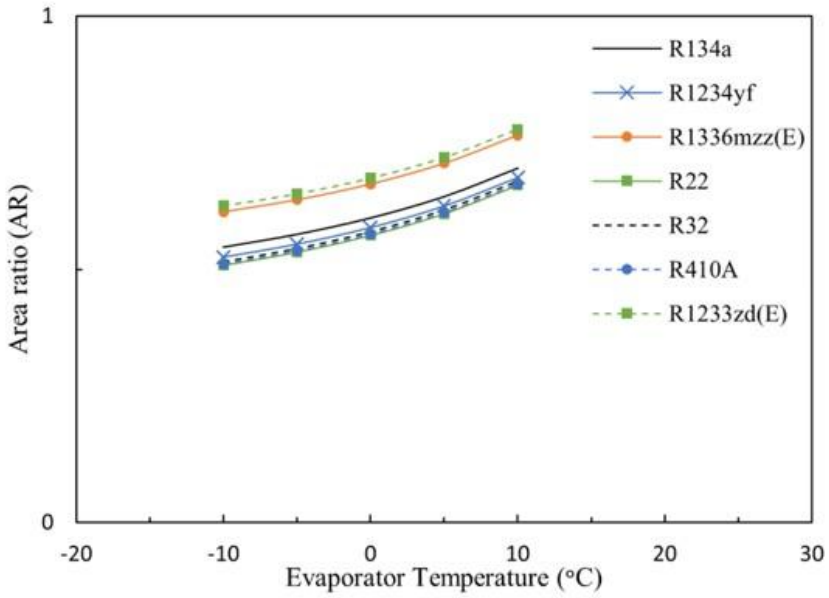


Fig. 6: The ECU's area ratio against the evaporator temperature

Increasing the evaporator temperature increases the compressor suction pressure. Since the condenser pressure remains constant under the specified conditions, the compressor pressure difference decreases. As a result, the compressor piston requires less driving force. The expander-side pressure difference remains essentially unchanged, so a smaller expander area is sufficient to drive the fixed compressor area, resulting in a higher area ratio.

The findings suggest that refrigeration at low temperatures constitutes the most challenging mechanical operating condition. At T_{evap} = -10°C, the low suction pressure produces a large compression pressure difference and requires a comparatively large expander piston. A unit designed only for air-conditioning duty near 10 °C may therefore fail to provide sufficient driving force when used for freezing or low-temperature preservation. Possible consequences include incomplete compression, reduced discharge mass flow, failure to open the discharge valves, short piston strokes, or complete piston stalling. The comparatively slight variation among most fluid curves indicates that the evaporator temperature exerts a similar influence on compressor load across all working fluid candidates. Nonetheless, even slight changes in AR may matter in a free-piston machine, as no crankshaft or electric motor can drive the piston through the more demanding phases of the cycle.

3.1.2 Combined interpretation and practical design implications

The above discussion indicates that a single fixed area ratio cannot achieve precise force matching across the entire operating envelope. Higher generator temperature increases the area ratio (AR), while higher condenser temperature significantly reduces it. In contrast, increasing evaporator temperature moderately increases AR. The most challenging scenario for generating adequate driving force is anticipated when the generator temperature is low, the condenser temperature is high, and the evaporator temperature is low. Conversely, high generator temperature, low condenser temperature, and high evaporator temperature can result in excessive driving force and piston acceleration. For practical implementation, the selected geometry should satisfy two limits:

- At the minimum available expansion force, the piston must still overcome compression, friction, valve pressure drops, seal resistance, and auxiliary loads.
- At the maximum expansion force, piston velocity and stroke must remain within acceptable limits without collision, excessive vibration, or unstable valve operation.

If the predicted AR range is too wide for fixed geometry, practical control strategies could include variable expander admission timing, adjustable clearance volume, generator-pressure regulation, a controllable bypass, or an auxiliary gas spring. These measures could maintain piston motion as waste-heat and cooling-load conditions change. Overall, the area-ratio analysis is one of the most practically significant results of this work. It transforms thermodynamic operating conditions into a directly usable mechanical-design requirement. This means that optimization based only on COP is insufficient. The final system design should therefore optimize working-fluid selection, COP, cooling capacity, operating pressure, and the feasible piston-area-ratio envelope simultaneously.

3.2 Thermodynamic performance of the ORC-VCC-based ECU

This section examines the ORC-VCC from a thermodynamic performance perspective, after confirming that the ECU area ratio (AR) is feasible for operation. It evaluates generator temperatures of 60–90 °C, condenser temperatures of 30 – 45 °C, and evaporator temperatures of −10 – 10 °C. The parameters of interest are external generator heat input (Qgen), evaporator cooling capacity (Qevap), and the system COP. This definition quantifies the conversion of supplied heat into useful cooling.

3.2.1 Effect of generator temperature on system performance

3.2.1.1 Generator heat input

The influence of generator temperature was assessed at condenser temperature of 30°C and evaporator temperature of 10°C. Generator heat input, cooling capacity, and system COP must be considered concurrently, as generator temperature directly affects the ORC thermodynamic states and available expansion work, while the refrigeration-side temperatures remain constant. Fig. 7 illustrates the relationship between generator heat input and generator temperature. The findings identify three distinct groups of refrigerants. R32 and R410A exhibit the highest heat-input requirements, approximately 11 – 14 kW. R22 requires a moderate input, around 6.6–7.3 kW, whereas R134a and R1234yf necessitate about 5.0 – 6.1 kW. R1336mzz(E) and R1233zd(E) demonstrate considerably lower values, approximately 1.7 – 1.9 kW and 1.0 – 1.2 kW, respectively.

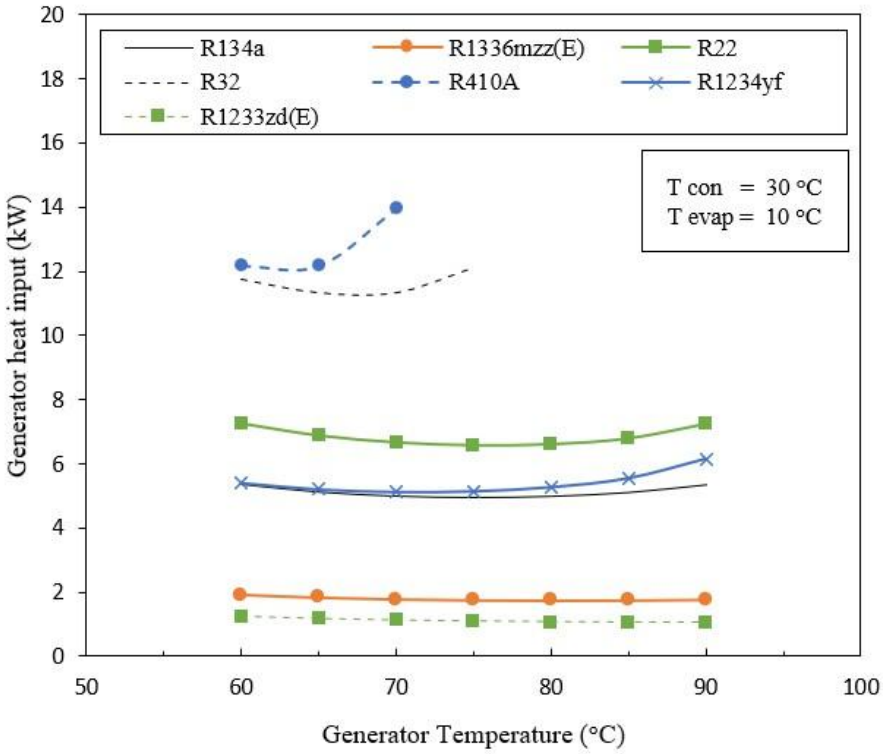


Fig. 7: The heat input against the generator temperature

These discrepancies cannot be attributed solely to the increase in generator enthalpy. In a reciprocating expander, the mass flow rate also depends on the refrigerant density at the suction port. Therefore, the mass flow rate can be expressed as:

$$\dot{m}_{\mathrm{ORC}} \approx (\rho_{\mathrm{exp,in}}\, \eta_{\mathrm{v,exp}} A_{\mathrm{exp}} L) N, \tag{21}$$

where $\rho_{\mathrm{exp,in}}$is the expander-inlet vapor density, L is the piston stroke, N is the operating frequency, and $\eta_{\mathrm{v,exp}}$is the volumetric efficiency.

Consequently, fluids with high vapor density or large required throughput can circulate significantly more mass per unit time (or a higher mass flow rate). Even when their specific generator enthalpy rise remains moderate, the resultant mass flow can generate a substantial total heat-input rate. This is why the high-pressure fluids R32 and R410A impose the highest generator duties.

Fig. 7 shows that most refrigerants exhibit a shallow U-shaped relationship between heat input and generator temperature. Initially, increasing the generator temperature reduces or only slightly changes the heat input. Higher generator pressure increases the available specific expansion work, and thus a smaller ORC mass flow is sufficient to provide the compressor-driving power. This reduction in required mass flow can initially offset the increased specific heat at the generator. Beyond a certain intermediate temperature, the heat input begins to rise. At this point, the increased heat requirement specific to the generator surpasses the reduction in mass flow. Additional superheating may also introduce heat without yielding a proportional increase in useful expansion work. Consequently, raising the heat-source temperature does not necessarily improve heat utilization. The minimum point on each curve indicates a balance between the heat supplied to the fluid and the mass flow required to operate the compressor.

R22 reaches its minimum heat input at approximately 75 to 80 °C, then increases up to 90 °C. R134a and R1234yf reach their minimum value at around 70 to 75 °C. R1336mzz(E) and R1233zd(E) show slight variation due to their low mass flow rate and heat-throughput levels. However, their low heat input does not indicate superior performance, as they also deliver significantly lower cooling capacities.

The R410A results terminate near 70 °C, whereas the R32 results are limited to approximately 75 °C. These limitations arise because their critical temperatures are close to the upper boundary of the investigated generator-temperature range. R410A has a critical region near 72 °C, while the critical temperature of R32 is approximately 78 °C. Above these temperatures, the conventional subcritical liquid–vapor phase boundary disappears. This limitation should be stated with caution. Although thermodynamic properties exist above the critical point, the current model and property-data methodology are designed for a subcritical Organic Rankine Cycle (ORC) with distinct evaporation and condensation stages. In the supercritical region, saturation-dependent quantities such as vapor quality and latent heat are no longer well-defined; furthermore, the generator functions as a single-phase supercritical heater rather than a traditional evaporator [31 – 33]. Therefore, the subcritical equations, state-point definitions, and property routines used in this analysis are not reliably applicable beyond the critical point. This may be further investigated in the next publication.

Therefore, the truncated R32 and R410A curves represent the valid range of the current subcritical model rather than a fundamental impossibility of operating these fluids at higher temperatures. Modeling such operation would require a dedicated transcritical formulation, pressure optimization independent of saturation temperature, and property data that accurately capture the large variations in specific heat and density near the pseudocritical region. Directly connecting the present curves to hypothetical supercritical points could otherwise produce discontinuities or physically misleading performance trends.

3.2.1.2 Cooling capacity

The cooling-capacity curves are independent of the generator variations, as shown in Fig. 8. R32 provides the largest capacity at approximately 5.9 kW, followed by R410A at about 5.5 kW and R22 at approximately 3.7 kW. R134a and R1234yf produce approximately 2.4 and 2.3 kW, respectively, whereas R1336mzz(E) and R1233zd(E) provide approximately 0.75 and 0.52 kW. This behavior is caused by fixed condenser and evaporator temperatures; therefore, the refrigeration effect per unit mass remains unchanged for each fluid. Moreover, the compressor piston area, stroke, and operating frequency are also fixed. Under constant volumetric efficiency and swept volume, the refrigerant mass flow rate remains unchanged. Changes in generator temperature affect the pressure force available from the expander and the required expander area, but they do not directly alter the VCC state points or compressor displacement.

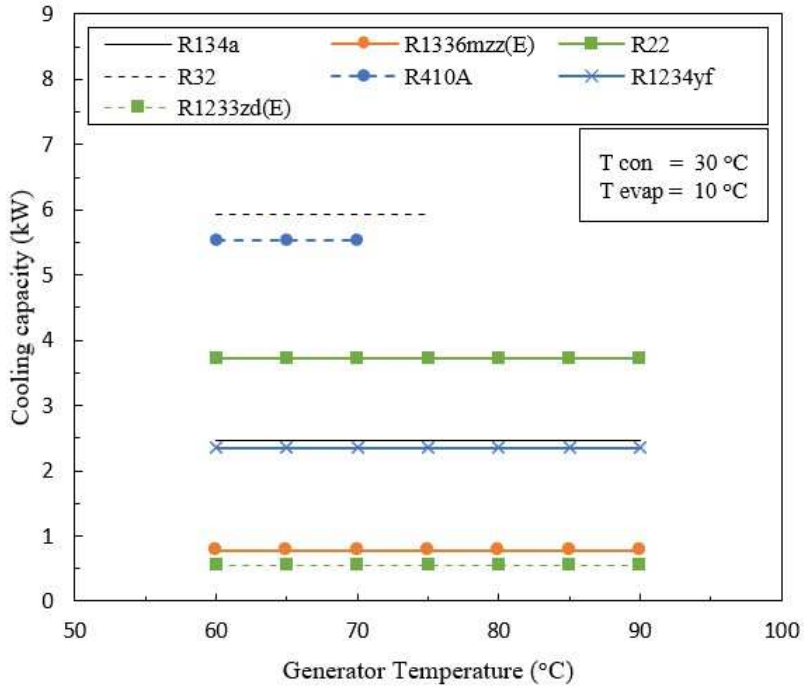


Fig. 8: The cooling capacity against the generator temperature

The result shows a clear difference between driving potential and cooling capacity. Raising generator temperature supplies higher-grade thermal energy and changes the required mechanical matching, but it does not increase cooling capacity when compressor swept volume and refrigeration-side temperatures are fixed. Under these assumptions, increasing heat source temperature to obtain more refrigeration would therefore be ineffective. A higher cooling load requires a larger compressor swept volume, increased operating frequency, improved volumetric efficiency, or a fluid with greater volumetric refrigeration capacity (or higher density).

R32 and R410A achieve high capacities due to their high suction-vapor density and favorable volumetric refrigeration capacity. In contrast, low-pressure fluids such as R1233zd(E) and R1336mzz(E) deliver less mass flow through the compressor at the same displacement, resulting in significantly lower cooling rates. When using these fluids, consider their low generator capacities alongside the need for increased displacement to achieve comparable cooling effectiveness.

In a real free-piston machine, cooling capacity may vary with generator temperature. Changes in piston frequency, stroke, valve timing, leakage, volumetric efficiency, and oscillation stability can indirectly affect compressor throughput. Therefore, the constant-capacity result applies only under the current fixed-displacement, steady-state assumptions.

3.2.1.3 Coefficient of performance

Because cooling capacity is approximately independent of generator temperature, the shape of each COP curve is governed mainly by the inverse variation of generator heat input. The system COP against the generator temperature under various working fluids is shown in Fig. 9

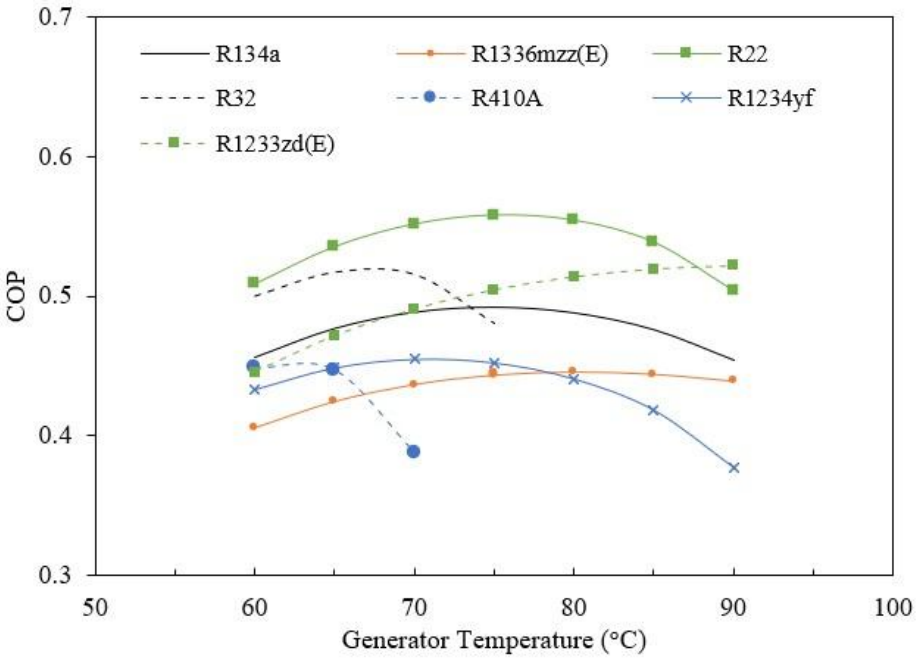


Fig. 9: The system COP against the generator temperature

Fig. 9 shows that most fluids exhibit a maximum Coefficient of Performance (COP) near the temperature at which their generator heat input is minimized. R22 shows the highest peak COP, increasing from about 0.51 at 60 °C to about 0.56 at 75 °C before declining to roughly 0.50 at 90 °C. The COP reaches its maximum when the increase in specific expansion work initially surpasses the generator's additional heat requirement. At higher generator temperatures, increased generator duty does not provide extra cooling, causing the COP to decrease.

R134a exhibits a comparable, though less pronounced, response, attaining a broad maximum of approximately 0.49 near 70–75 °C before decreasing. The broad nature of this maximum is operationally advantageous, as moderate fluctuations in waste-heat temperature have only a limited impact on performance near the optimum. R1234yf reaches a maximum COP of approximately 0.45 at around 70 °C and subsequently declines markedly toward 90 °C. This trend indicates that, under the specified conditions, additional high-temperature heat is converted into useful expansion work less effectively.

The COP produced by R1336mzz(E) increases gradually to approximately 0.44–0.45, and, then it stabilizes. This reflects slight changes in heat input and cooling capacity. In contrast, R1233zd(E) shows a steady COP increase from about 0.45 to 0.52 across the investigated range. Its generator heat input decreases slightly while cooling capacity remains constant, resulting in a continuous increase in COP. The lack of a maximum within the generator temperature interval suggests the optimum is at or beyond the upper boundary of the evaluated subcritical range.

R32 and R410A must be interpreted within their restricted temperature range. R32 exhibits a maximum COP near 65–70 °C and then declines as the critical region is approached. R410A shows an even narrower useful range and a significant reduction near its critical point. Near the critical point, the latent heat of vaporization approaches zero and its saturation properties become highly nonlinear. Slight temperature changes can cause large variations in density, specific heat, and required pressure. These effects make performance and numerical predictions highly sensitive to the selected generator pressure. Thus, the last subcritical data point should not be interpreted as evidence of the subsequent transcritical trend.

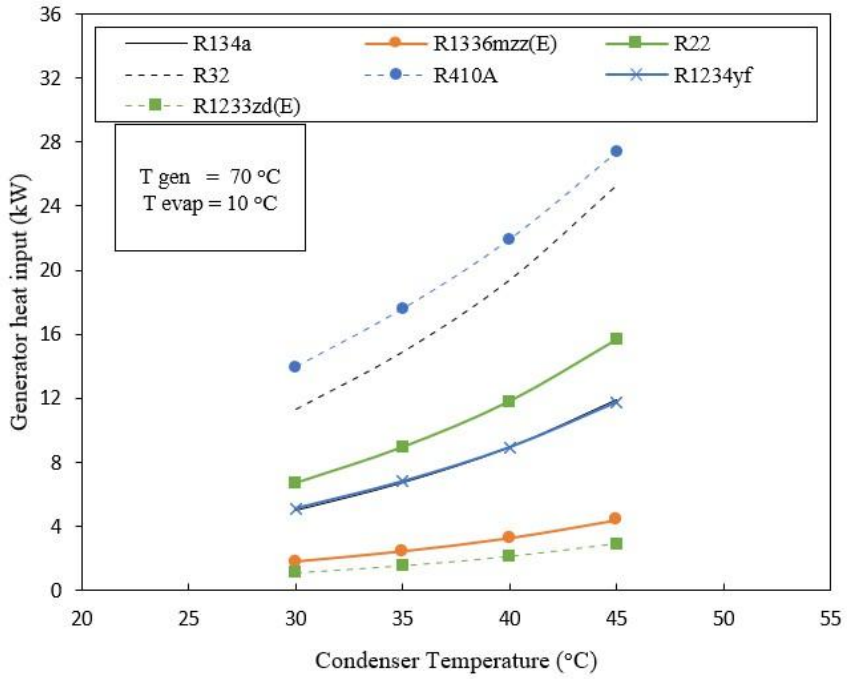
The results show that the highest generator temperature is not always the most efficient operating condition. An optimal point balances increasing specific expansion work with increasing heat supplied per unit

mass. Since the cooling capacity is displacement-controlled in this model, heat supplied above the optimum raises thermal consumption without adding refrigeration. R22 provides the highest theoretical COP throughout the investigated range, but its ozone-depletion potential makes it unsuitable for new systems, and it should be kept only as a performance benchmark. R32 and R410A offer high cooling capacity per unit displacement but require large generator duties and are limited by their low critical temperatures. R1233zd(E) has the highest COP at the upper end of the range but delivers relatively low capacity for the same compressor geometry. Fluid selection must balance COP, absolute cooling output, waste-heat availability, piston displacement, operating pressure, environmental impact, safety, and proximity to the critical region.

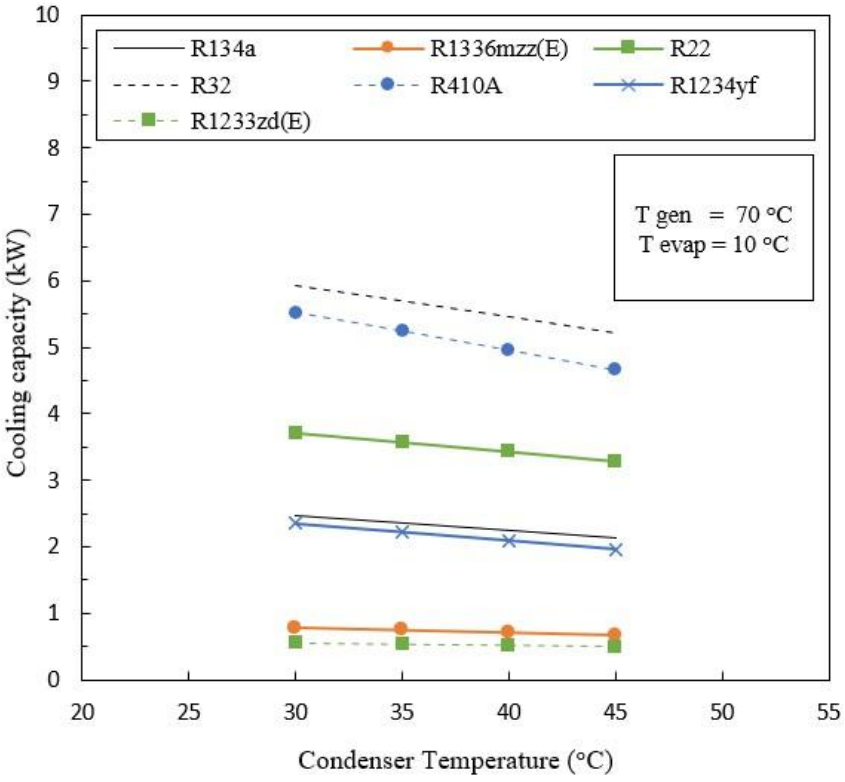
For practical control, the generator should operate near the fluid-specific COP maximum rather than the maximum available waste-heat temperature. If the heat source temperature is higher than needed, mass-flow control, bypass regulation, or a recuperative arrangement may work better than simply increasing the generator temperature. Experimental validation should quantify expander efficiency, piston dynamics, valve losses, heat-exchanger pressure drops, and auxiliary consumption because these factors may shift the optimum from that predicted by the idealized steady-state model.

3.2.2 Effect of condenser temperature on system performance

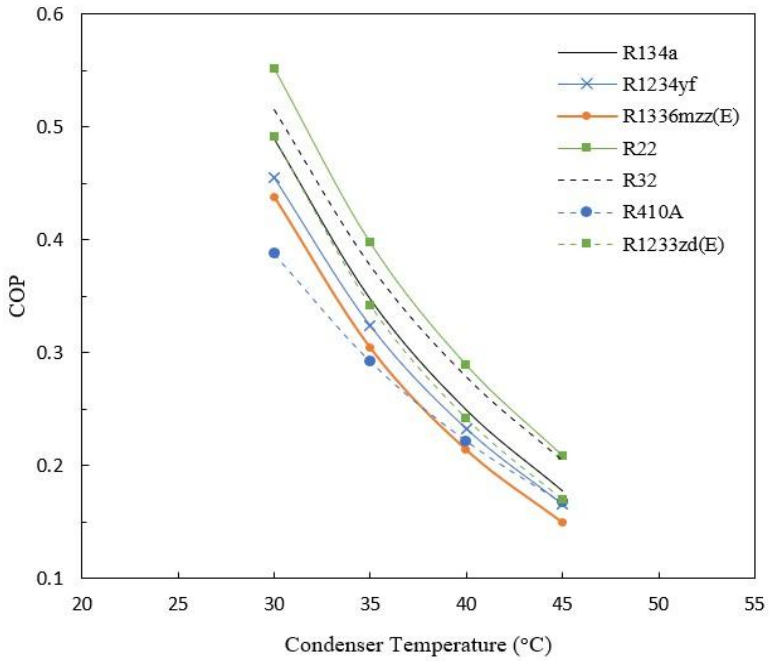
The influence of condenser temperature was investigated from 30 to 45 °C while maintaining the generator and evaporator temperatures at 70 and 10 °C, respectively. Fig. 10 shows the results. Condensation temperature is one of the most influential operating parameters of the proposed thermally driven ORC–VCC system. Increasing condensation temperature reduces the cooling capacity; at the same time, the generator requires higher heat input. This markedly reduces the overall coefficient of performance. This is because the condenser pressure (at the condensation temperature) affects both sides of the mechanically coupled ECU. On the refrigeration side, higher condenser pressure increases the reaction force on the compressor's piston that the compressor must overcome. On the ORC side, higher condenser pressure raises expander back pressure and reduces the pressure difference available to drive the free piston. Consequently, an increase in condenser temperature imposes a compounded thermodynamic penalty rather than solely impacting the heat rejection process.



(a) Generator heat input against the condenser temperature



(b) Cooling capacity against the condenser temperature



(c) COP against the condenser temperature

Fig. 10: The generator heat input, cooling capacity, and COP against the condenser temperature

Fig. 10 also shows that cooling capacity decreases consistently with increasing condenser temperature for all refrigerants. As the condenser temperature increases, the condensation pressure and saturated-liquid enthalpy at the condenser outlet increase. Because the throttling process is isenthalpic, the refrigerant then enters the evaporator with a higher enthalpy. The specific cooling capacity is reduced. A higher compressor pressure ratio can reduce effective refrigerant delivery by increasing clearance-volume re-expansion and internal leakage. These mechanisms explain the progressive decline in cooling capacity. R32 and R410A maintain the highest cooling capacities because their relatively high suction-vapor densities provide higher volumetric refrigeration capacity. Thus, a fixed compressor swept volume circulates a comparatively larger mass flow rate. However, this advantage comes with higher operating pressure and a much larger generator heat input. In contrast, R1233zd(E) and R1336mzz(E) produce much lower capacity for the same compressor geometry. These fluids would require a larger compressor displacement or higher operating frequency to provide a cooling duty comparable to that of R32 or R410A. The approximately 10 – 17% reduction in cooling capacity across the investigated condenser-temperature range is moderate compared with the increase in generator heat input. Nevertheless, it is practically significant because the useful output decreases precisely when the system requires substantially more thermal energy.

Generator heat input increases nonlinearly with condenser temperature for every refrigerant. The sharp increase in $\dot{Q}_{\mathrm{gen}}$is primarily related to the mechanical coupling condition. At a fixed generator temperature, increasing T_{con}raises P_{con}. This produces two simultaneous effects: 1) The available expander pressure difference, $P_{\mathrm{gen}} - P_{\mathrm{con}}$, decreases; and 2) the compressor pressure difference, $P_{\mathrm{con}} - P_{\mathrm{evap}}$, increases. Thus, the expander has less pressure potential available while the compressor requires more work. To maintain piston motion, the system must increase the expander-side force, displacement, mass throughput, or effective piston area. In the present model, the resulting mechanical matching causes the required ORC flow and generator heat input to increase sharply. The nonlinear growth of $\dot{Q}_{\mathrm{gen}}$is consistent with the nonlinear saturation-pressure relationship.

This result is especially important for waste-heat utilization. A system sized using the generator duty at $T_{\mathrm{con}} = 30°\mathrm{C}$ may not receive sufficient thermal power to operate continuously at 40–45 °C. Under these

conditions, the free piston may experience a shorter stroke, lower frequency, incomplete compression, or complete stalling unless the expander–compressor geometry and control system have been designed for the adverse condition. Although R1233zd(E) and R1336mzz(E) have the lowest heat demands, they show large relative increases as condenser temperature rises. Therefore, a quite low generator heat input should not be taken as low sensitivity. The fractional increases in heat input, cooling output, and machine displacement must be evaluated together.

As condenser temperature increases, cooling capacity decreases and heat input rises, resulting in a sharper decline in COP than either factor alone. All refrigerants experience a significant COP drop from 30 to 35 °C, with further reduction up to 45 °C. The convergent trend at high condenser temperature shows that poor heat rejection can outweigh the thermodynamic benefits of specific refrigerants. Selecting a high-performance refrigerant cannot fully compensate for a poorly designed condenser. R22 remains a strong theoretical performer, but due to its ozone-depletion potential, it should be considered a legacy reference, not a candidate for new equipment.

R32 provides high cooling capacity and reasonable COP at low condenser temperatures. However, the generator heat demand increases significantly with the condenser temperature. R410A also produces high cooling capacity, but its high heat-input requirement results in a lower COP. R1233zd(E) maintains low generator duty and competitive COP, but offers quite low cooling capacity for the specified displacement. These results show that selecting a refrigerant based solely on COP is insufficient. It also considers the cooling capacity, generator size, pressure containment, environmental impact, and piston dimensions.

Thermodynamic interpretation and practical implications

Condensation temperature affects both thermodynamic efficiency and mechanical feasibility. It should be operated as low as possible. This is because maintaining a low condensation temperature provides several simultaneous advantages:

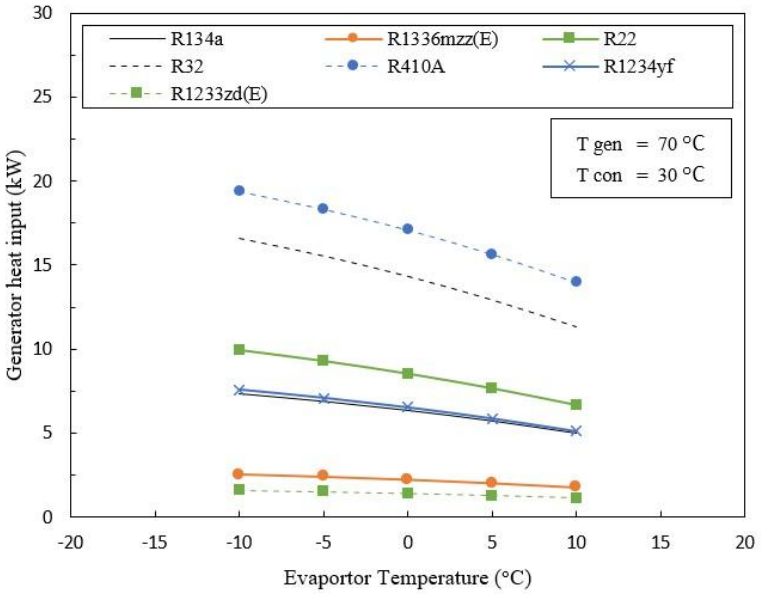
- higher cooling capacity;
- lower compressor pressure ratio;
- greater ORC expander pressure difference;
- lower generator heat demand;
- higher system COP;
- a less demanding expander–compressor area ratio; and
- improved margin against piston stalling.

For effective implementation, the condenser must be designed to operate at the expected ambient or coolant temperature. Key considerations include heat-transfer area, coolant flow rate, fan or pump control, refrigerant charge, fouling resistance, and condenser approach temperature. In hot climates, evaporative or water-cooled cooling towers offer advantages. The evaluation should include water usage and auxiliary energy consumption.

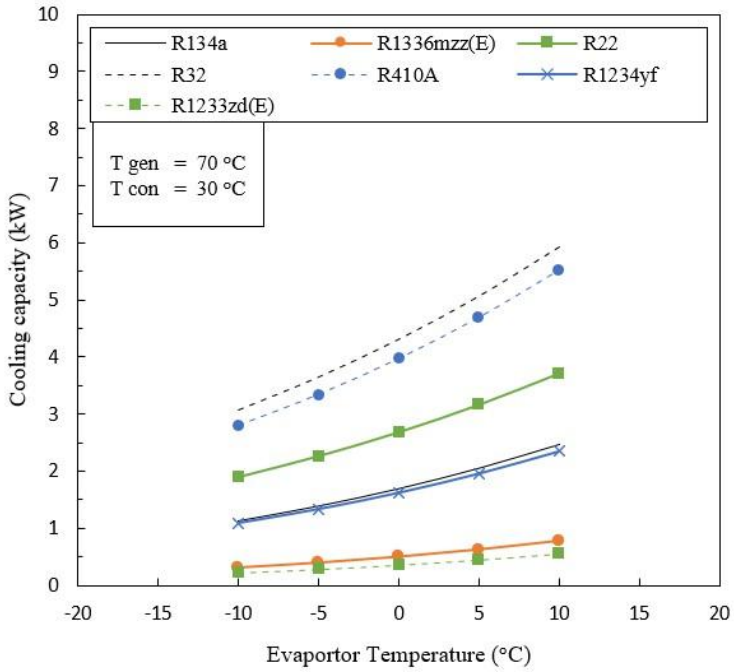
In a practical ECU, increased discharge pressure can raise valve pressure losses, leakage, mechanical friction, discharge temperature, and dynamic instability. These factors cause greater performance deterioration than the idealized model predicts. Experimental validation should include measurements of instantaneous cylinder pressure, piston displacement, mass flow, condenser heat rejection, and auxiliary electrical consumption across the entire condenser-temperature range. Overall, condenser temperature is a key system-level constraint. Higher condenser temperatures weaken the ORC driving process, increase VCC compression requirements, reduce useful refrigeration, and raise external heat consumption. Effective heat rejection is therefore essential for efficient and stable operation of the proposed directly coupled ORC–VCC system.

3.2.3 Effect of evaporator temperature on system performance

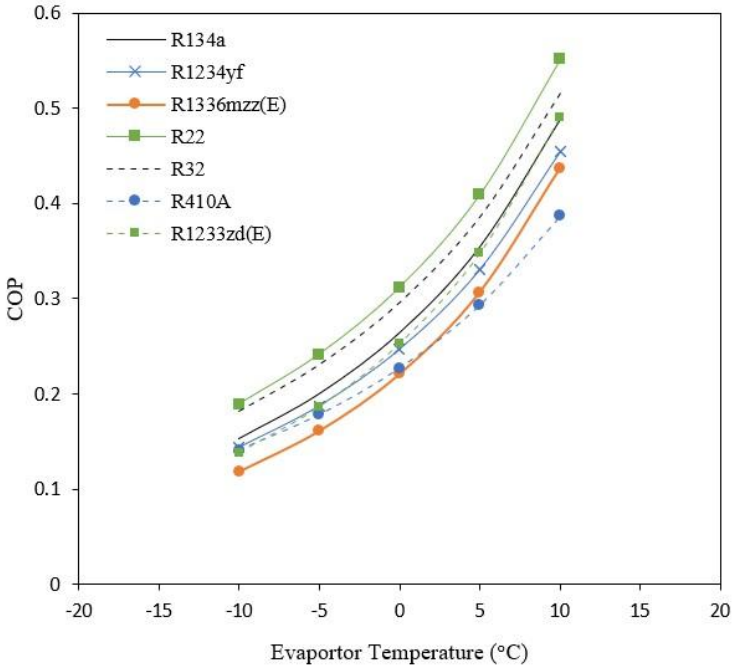
The effect of evaporator temperature T_{evap}, was investigated, ranging from −10 to 10 °C while maintaining $T_{\text{gen}} = 70°\text{C}$ and $T_{\text{con}} = 30°\text{C}$. Increasing T_{evap}improves all three performance indicators: cooling capacity increases, generator heat input decreases, and COP rises substantially. These simultaneous improvements arise primarily from the increase in evaporating pressure and the corresponding reduction in compressor pressure ratio.



(a) Generator heat input against the evaporator temperature



(b) Cooling capacity against the evaporator temperature



(c) COP against the evaporator temperature

Fig. 11: The generator heat input, cooling capacity and the COP against the evaporator temperature

Cooling capacity increases nonlinearly with evaporator temperature for every refrigerant. From −10 to 10 °C, R32 increases from approximately 3.1 to 5.9 kW, while R410A increases from about 2.8 to 5.5 kW. R22 rises from approximately 1.9 to 3.7 kW. R134a and R1234yf increase from approximately 1.1 kW to 2.4 kW, whereas R1336mzz(E) and R1233zd(E) remain below 1 kW. As T_{evap}increases, suction pressure and vapor density rise. For a fixed compressor displacement, the higher suction density increases the refrigerant mass circulated per stroke. The refrigeration effect per unit mass also changes with the evaporator state. Therefore, the capacity increase should be attributed to the combined effects of suction density, mass-flow rate, and evaporator enthalpy difference—not solely to latent heat.

R32 and R410A provide the highest capacities because of their high volumetric refrigeration capacities. However, this advantage is accompanied by high generator heat requirements and operating pressures. Conversely, R1233zd(E) and R1336mzz(E) require less heat but would need a larger compressor displacement to deliver the same cooling duty.Generator heat input decreases continuously as T_{evap}rises. For example, R410A decreases from approximately 19.3 to 14.0 kW, R32 from 16.6 to 11.3 kW, and R22 from 9.8 to 6.7 kW. R134a and R1234yf decline to approximately 5.1 kW at 10 °C. R1233zd(E) maintains the lowest requirement, decreasing from about 1.6 to 1.1 kW. This trend is explained by the decreasing compressor pressure lift. At constant condenser temperature, raising T_{evap}increases P_{evap}, thereby reducing both the pressure difference and pressure ratio across the compressor. Consequently, less compression work is required per unit mass. The mechanically coupled expander must therefore supply less power, reducing the ORC mass flow and external heat input required in the generator.

This result highlights the difficulty of low-temperature refrigeration. At −10 °C, the compressor experiences a large pressure ratio, while suction-vapor density and cooling capacity are relatively low. Consequently, the system requires more thermal input to produce less refrigeration. These conditions also impose a greater mechanical load on the free-piston assembly and increase the risk of insufficient stroke or piston stalling.

Fig. 11 also shows that COP increases rapidly and nonlinearly. R22 rises from approximately 0.19 at −10 °C to 0.55 at 10 °C and produces the highest theoretical COP. R32 reaches approximately 0.51, while R1233zd(E) approaches 0.49. R1234yf, R1336mzz(E), and R410A reach approximately 0.46, 0.44, and 0.39, respectively. Overall, evaporator temperature depends on the application. The system described is more thermodynamically optimized for moderate-temperature refrigeration rather than for deep-freezing tasks. Refrigerant selection should therefore be based on the intended evaporator temperature rather than a single reference condition, considering COP, volumetric cooling capacity, heat-source temperature, piston displacement, operating pressure, and environmental acceptability simultaneously.

3.3 Effect of piston stroke length on system performance

This section discusses the effect of stroke length on system performance. It is demonstrated under fixed generator, condenser, and evaporator temperatures of 70, 30, and 10°C, respectively. The piston stroke length, L, directly determines the swept volume of the free-piston expander–compressor and therefore controls the mass flow rates, cooling capacity, and generator heat requirement. For a reciprocating chamber, the displaced volume per stroke is:

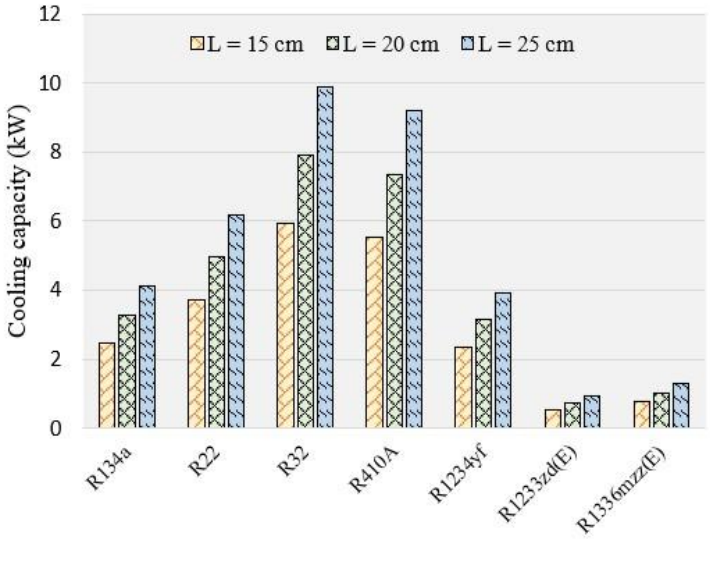
$$V_{\mathrm{s}} = A_{\mathrm{exp}} L, \tag{22}$$

where $A_{\mathrm{exp}}$is the expander cross-sectional area. The mass-flow rate can therefore be expressed as

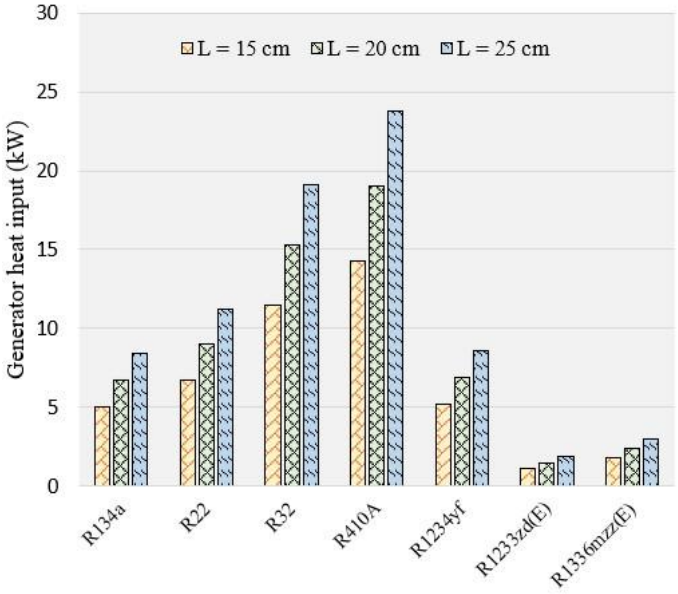
$$\dot{m} \approx \rho\, \eta_{\mathrm{v}} A_{\mathrm{exp}} L N \tag{23}$$

where ρ, η_v, and f represent the inlet density, volumetric efficiency, and operating frequency, respectively. When these quantities and the thermodynamic state points are fixed, mass flow is directly proportional to piston stroke.

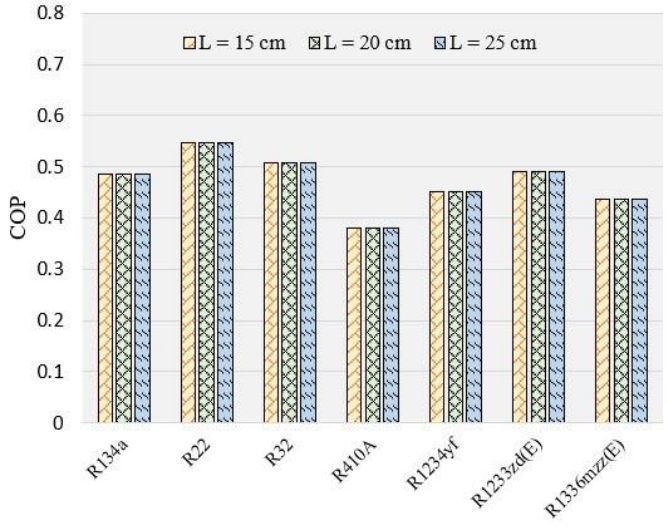
Fig. 12a depicts variations in cooling capacity with stroke length among working fluids. The cooling capacity of all working fluids increases with the stroke length. Increasing the stroke from 15 to 25 cm represents a 66.7% increase in swept volume and produces a proportionally larger capacity increase. R32 exhibits the highest cooling capacity, rising from about 5.9 to 9.8 kW, followed by R410A, which increases from approximately 5.5 to 9.2 kW. R22 rises from about 3.7 to 6.2 kW, whereas R134a and R1234yf increase from approximately 2.4 to 4.1 kW and from 2.3 to 3.9 kW, respectively. R1233zd(E) and R1336mzz(E) provide lower capacities because of their lower volumetric refrigeration capacities.



(a)



(b)



(c)

Fig. 12: The heat input, cooling capacity, and COP when varying the stroke length

Since the evaporator and condenser conditions remain unchanged, the refrigerating effect per unit mass is unchanged. Thus, the increase in $\dot{Q}_{\text{evap}}$is primarily caused by the greater refrigerant mass displaced during each stroke. The piston stroke consequently acts as a capacity-scaling parameter rather than as a variable that improves the underlying refrigeration cycle.

Generator heat input also increases with the stroke length. R410A has the highest thermal requirement, increasing from approximately 14.1 kW at $L = 15$ cm to 23.7 kW at $L = 25$ cm. R32 rises from about 11.5 to 19.0 kW, while R22 increases from approximately 6.7 to 11.2 kW. The heat-input requirements of R1233zd(E) and R1336mzz(E) remain considerably lower, although they increase proportionally with stroke. A longer stroke length increases expander displacement and ORC mass throughput. Consequently, more working fluid must be heated and vaporized per unit time, increasing the generator duty. The nearly linear trend indicates that the state-point enthalpy difference and component efficiencies were assumed to remain constant as the machine was scaled.

The result has an important practical implication. Although increasing piston stroke can provide greater cooling capacity, it requires more heat input to operate the system. This may be limited by the available waste-heat source and heat transfer rate. If the available heat or heat-transfer conductance is insufficient, the expander-inlet temperature, pressure, or vapor quality may decrease, and the predicted linear capacity increase will not be achieved.

Fig. 12c also shows that the COP remains nearly constant for each refrigerant at all three stroke lengths because cooling capacity and generator heat input increase in essentially the same proportion. Thus, increasing stroke length increases system throughput without changing ideal thermodynamic efficiency. R22 has the highest theoretical COP at approximately 0.54, followed by R32 at approximately 0.50. R134a and R1233zd(E) are close to 0.48 – 0.49, while R410A gives the lowest value, approximately 0.38.

The constant COP reflects the steady-state model rather than a universal characteristic of real free-piston machines. In practice, longer strokes increase mean and peak piston velocity, seal travel, frictional dissipation, vibration, and the risk of piston impact. They can also affect valve timing, leakage, heat transfer, clearance-volume re-expansion, and oscillation stability. These losses do not necessarily scale linearly with stroke and may cause an optimum stroke to emerge experimentally.

Overall, piston stroke effectively matches system capacity to the required cooling load, but it does not inherently improve COP. Its selection should balance cooling output, available waste-heat rate, generator and evaporator dimensions, machine length, piston dynamics, structural stress, seal durability, and stable operating limits. Experimental or dynamic optimization is therefore required before applying the linear scaling predicted by the ideal model to prototype design.

3.4 Effect of piston operating frequency on system performance

The stroke frequency (N) directly relates to the volumetric throughput of the mechanically coupled expander–compressor. It represents individual piston strokes rather than complete reciprocating cycles; one full cycle consists of two strokes. In this section, the effect of increasing the stroke frequency from 2 to 4 strokes/s. The generator, evaporator, and condenser temperatures are held constant at 70, 10, and 30 °C, respectively. The results are shown in Fig. 13.

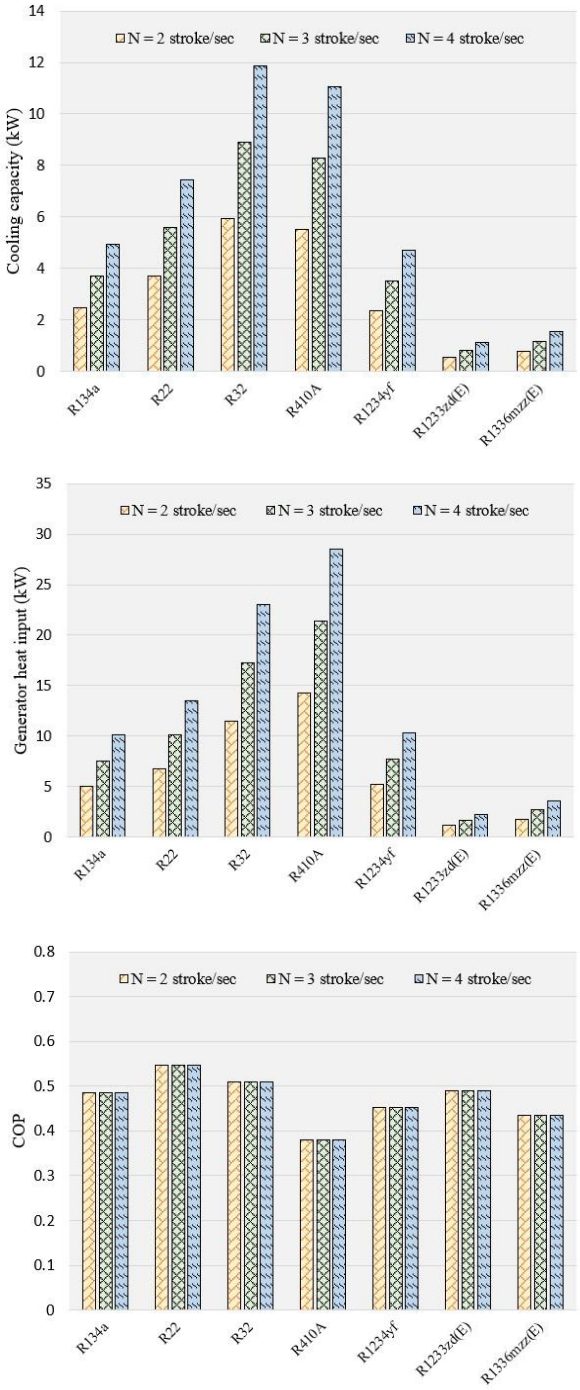


Fig. 13: The heat input, cooling capacity, and COP when varying the operating frequency

Fig. 13a shows that cooling capacity increases almost linearly with stroke frequency. As the frequency rises from 2 to 4 strokes per second, the cooling capacity of R32 increases from approximately 5.9 to 11.8 kW, while R410A increases from about 5.5 to 11.0 kW. R22 increases from approximately 3.7 to 7.4 kW. The capacities of R134a and R1234yf increase from approximately 2.4 to 4.9 kW and from 2.3 to 4.7 kW, respectively. Although R1233zd(E) and R1336mzz(E) provide lower capacities, they exhibit a similar proportional response.

Because the evaporator and condenser conditions remain unchanged, the specific refrigeration effect is constant for each fluid. Therefore, the increase in cooling capacity results primarily from the higher refrigerant mass flow rate. Frequency is consequently an effective capacity-control parameter: cooling output can be adjusted without changing piston or cylinder geometry. The differences among the fluids reflect their volumetric

refrigeration capacities. R32 and R410A provide high cooling product because a fixed compressor displacement circulates a relatively large refrigerant mass. The lower-pressure fluids R1233zd(E) and R1336mzz(E) produce less cooling for the same swept-volume rate and would require greater displacement or frequency to achieve an equivalent duty.

Generator heat input also increases almost directly with frequency as shown in Fig. 13b. R410A has the highest requirement, increasing from approximately 14.2 kW at 2 strokes/s to 28.5 kW at 4 stroke/s. R32 rises from approximately 11.5 to 23.0 kW, while R22 increases from about 6.7 to 13.4 kW. R1233zd(E) has the lowest generator duty, increasing from approximately 1.0 to 2.0 kW. A higher operating frequency increases the ORC side mass flow rate. More fluid must therefore be heated and vaporized in the generator to maintain the specified expander-inlet condition. This requires higher heat input to the generator. If the heat input is not satisfied, the inlet temperature or vapor quality will decline, reducing the available expansion force and preventing the expected capacity increase.

Since both cooling capacity and generator heat demand increase in approximately the same proportion, the COP of each working fluid is independent of the stroke frequency as seen in Fig. 13c. R22 provides the highest theoretical COP at approximately 0.54, followed by R32 at about 0.50. R134a and R1233zd(E) produce values near 0.48–0.49, whereas R410A gives the lowest COP at approximately 0.38. At higher frequencies, piston velocity and acceleration increase, shortening the available time for valve opening, chamber filling, heat transfer, and pressure equalization. Valve pressure losses, flow choking, leakage, seal friction, vibration, and inertial forces may consequently increase. Volumetric efficiency may fall if the suction chamber cannot fill completely, while delayed discharge-valve opening can cause over-compression. These effects would cause cooling capacity to increase less than proportionally and may increase generator input disproportionately, producing an optimum practical frequency. Overall, operating frequency offers a flexible way to control cooling capacity, but higher frequency requires a proportional increase in available waste heat and more demanding mechanical and valve performance. Prototype optimization should therefore consider piston dynamics, resonant behavior, valve response, heat-exchanger conductance, pressure fluctuations, and fatigue limits rather than selecting the maximum achievable frequency based solely on ideal linear trends.

3.5 Overall synthesis, limitations, and research needs

Across all cases, the analysis's principal contribution is the explicit connection between thermodynamic boundary conditions and the geometry of a directly coupled expander–compressor. Generator temperature controls the available expansion pressure, condenser temperature penalizes both cycles simultaneously, and evaporator temperature governs compressor lift. The required area ratio captures their combined effect, while stroke and frequency mainly scale throughput. This separation of force matching, capacity scaling, and thermal efficiency provides a rational design sequence: first establish a feasible AR envelope, then select the swept-volume rate for the target load, and finally minimize external heat input through operating-point optimization and recuperation.

The fluid comparison further shows that high absolute cooling capacity, low generator duty, and high COP are not equivalent objectives. High-pressure fluids can deliver high volumetric capacity but impose larger heat duties and pressure containment requirements. Low-pressure fluids reduce heat throughput but generally require larger displacement for the same capacity. R1233zd(E) is especially promising in the modeled favorable-temperature region, whereas R22 should remain a performance benchmark rather than a recommended new-system choice. A final fluid decision requires a multi-objective assessment including safety, environmental regulation, stability, lubricity, leakage consequences, and component size.

The reported values are theoretical predictions and should be interpreted within the model boundary. Isentropic efficiencies, volumetric efficiency, pressure drops, heat leakage, valve timing, clearance-volume re-expansion, seal friction, piston inertia, and transient chamber pressures can materially alter both the self-oscillation condition and the net COP. Recuperator effectiveness and pinch constraints also need explicit

treatment. The next step should combine a time-resolved dynamic model with prototype measurements of cylinder pressure, displacement, frequency, mass flow, heat-transfer rates, and auxiliary electricity. Uncertainty propagation and exergy analysis would then identify whether observed losses arise principally in heat exchange, expansion/compression, throttling, or mechanical transmission. Such validation is essential before using the present trends for scale-up or techno-economic comparison with absorption and electrically driven refrigeration technologies.

4. Conclusions

This study developed and applied a thermodynamic framework for evaluating a waste-heat-driven combined organic Rankine cycle–vapour compression cycle (ORC–VCC) equipped with a directly coupled free-piston expander–compressor unit (ECU). The proposed configuration can convert low-grade thermal energy directly into refrigeration. Direct mechanical coupling consequently reduces the number of energy-conversion stages and offers a potentially compact solution for waste-heat-driven cooling applications. The principal conclusions are summarized as follows:

- The piston-area ratio is a governing ECU design parameter rather than merely a geometric specification. It determines whether the pressure force generated on the ORC side is sufficient to overcome the compressor pressure load, mechanical resistance, and other parasitic losses throughout the piston stroke.
- Increasing the condenser temperature substantially reduced the required area ratio under the investigated force-balance formulation. Nevertheless, this geometric effect should not be interpreted as a thermodynamic benefit. A higher condensing temperature increased the generator heat requirement, reduced the cooling capacity, and caused a pronounced deterioration in the system COP because both the ORC back pressure and the VCC compression load increased.
- Raising the evaporator temperature increased the cooling capacity and system COP while decreasing the generator heat input. This improvement resulted mainly from higher compressor suction pressure, a reduced compression ratio, greater refrigerating effect, and lower work required per unit mass of refrigerant. The required area ratio also increased moderately, showing that improved cycle performance must be considered together with ECU force compatibility.
- Generator temperature produced a fluid-dependent optimum in COP. Although a higher temperature can increase the expansion work available to drive the compressor, it also raises the external heat supplied to the generator. Beyond the optimum range, the additional heat input is not converted into a proportional increase in cooling output; consequently, COP remains nearly constant or decreases. Generator temperature should therefore be optimized for each fluid rather than maximized indiscriminately.
- The working-fluid comparison revealed a distinct trade-off between cooling capacity and thermal efficiency. R32 and R410A produced comparatively high cooling capacities but also required large generator heat inputs. R22 provided the highest COP over much of the investigated range, although its ozone-depletion potential makes it unsuitable for new practical systems. The lower-GWP fluids R1234yf, R1233zd(E), and R1336mzz(E) offered environmentally preferable alternatives, but their lower volumetric capacities may require larger piston displacement or higher operating frequency.
- Performance results for R32 and R410A were restricted to conditions below their respective critical limits because the present formulation assumes subcritical evaporation and condensation. Results near the critical region should be interpreted cautiously because thermophysical properties become highly sensitive to temperature and pressure, and a transcritical formulation would be required beyond this boundary.

- Increasing the piston stroke increased both the displaced refrigerant volume and the mass processed during each cycle. Cooling capacity and generator heat input therefore increased almost proportionally with stroke. A similar result occurred when the piston operating frequency increased because more working cycles were completed per unit time.
- Under the steady-state idealized model, changes in stroke and operating frequency had little influence on COP because cooling capacity and generator heat input increased at approximately the same rate. In an actual ECU, however, this invariance is unlikely to be maintained at high speed or long stroke because valve-pressure losses, flow choking, leakage, piston friction, heat transfer, clearance re-expansion, vibration, and incomplete chamber filling become increasingly important.

The results demonstrate that selecting an ECU solely based on the highest predicted COP is insufficient. Practical design must simultaneously consider the required area ratio, piston stroke, operating frequency, pressure loading, mass-flow capacity, valve response, mechanical efficiency, seal performance, and the capability to maintain single-phase vapour at the expander and compressor inlets.

Overall, the study confirms the technical potential of a directly coupled ORC–VCC system for producing refrigeration from low-grade waste heat and establishes the piston-area ratio as the critical link between cycle thermodynamics and ECU implementation. The findings provide a basis for selecting working fluids, defining feasible operating ranges, and sizing a laboratory-scale prototype. Further work should extend the steady-state model to a time-resolved dynamic simulation incorporating chamber pressure evolution, valve dynamics, leakage, friction, clearance volume, transient heat transfer, and piston end-stop behavior. Experimental validation using compressed air, followed by testing with selected organic refrigerants, will be necessary to establish starting characteristics, stable oscillation limits, mechanical efficiency, and long-term ECU reliability.

Acknowledgments

This research was funded by King Mongkut's University of Technology North Bangkok, Contract no. KMUTNB-68-KNOW-05.

Declaration of competing interest

The authors declare that they have no known competing financial interests or personal relationships that could have appeared to influence the work reported in this paper.

Data availability

The data supporting the findings of this study are available from the corresponding author upon reasonable request.

References

1. Nikbakhti, R., Wang, X., & Chan, A. (2020). Performance analysis of an integrated adsorption and absorption refrigeration system. *International Journal of Refrigeration*, *117*, 269-283.
2. Jalili, M., Chitsaz, A., & Alhuyi Nazari, M. (2022). Investigating the fuel type influence on the thermo-economic performance of absorption refrigeration systems: a comparative study. *Journal of Thermal Analysis and Calorimetry*, *147*(7), 4763-4780.
3. Mungyeko Bisulandu, B. J. R., Mansouri, R., & Ilinca, A. (2023). Diffusion absorption refrigeration systems: an overview of thermal mechanisms and models. *Energies*, *16*(9), 3610.
4. Redhwan, A. A. M., Azmi, W. H., Sharif, M. Z., Mamat, R., Samykano, M., & Najafi, G. (2019). Performance improvement in mobile air conditioning system using Al2O3/PAG nanolubricant: AAM Redhwan et al. *Journal of Thermal Analysis and Calorimetry*, *135*(2), 1299-1310.

5. Kitrattana, B., Aphornratana, S., & Thongtip, T. (2023). Investigation on improvement potential of steam ejector performance in refrigeration cycle via constant rate of momentum change design method. *Applied Thermal Engineering*, *231*, 120953.
6. Yadav, V. K., Sarkar, J., & Ghosh, P. (2024). Recent advances and future outlook on solar-powered ejector refrigeration and associated multi-generation systems. *Journal of Thermal Analysis and Calorimetry*, 149(15), 7869-7889.
7. Nasir, M. T., Ekwonu, M. C., Esfahani, J. A., & Kim, K. C. (2021). Performance assessment and multi-objective optimization of an organic Rankine cycles and vapor compression cycle based combined cooling, heating, and power system. *Sustainable Energy Technologies and Assessments*, *47*, 101457.
8. Karellas, S., & Braimakis, K. (2016). Energy–exergy analysis and economic investigation of a cogeneration and trigeneration ORC–VCC hybrid system utilizing biomass fuel and solar power. *Energy conversion and management*, *107*, 103-113.
9. Wang, Z., Zhao, Y., Xia, X., Zhang, S., Xiao, Y., Zhang, X., & Chen, W. (2024). Experimental study of the thermodynamic performance of the ORC-VCC system with a zeotropic mixture. *Applied Thermal Engineering*, *250*, 123534.
10. Nasir, M. T., & Kim, K. C. (2016). Working fluids selection and parametric optimization of an Organic Rankine Cycle coupled Vapor Compression Cycle (ORC-VCC) for air conditioning using low grade heat. *Energy and Buildings*, *129*, 378-395.
11. Aphornratana, S., & Sriveerakul, T. (2010). Analysis of a combined Rankine–vapour–compression refrigeration cycle. *Energy Conversion and management*, *51*(12), 2557-2564.
12. Wang, H., Peterson, R., Harada, K., Miller, E., Ingram-Goble, R., Fisher, L., ... & Ward, C. (2011). Performance of a combined organic Rankine cycle and vapor compression cycle for heat activated cooling. *Energy*, *36*(1), 447-458.
13. Khan, Y., Raman, R., Rashidi, M. M., Said, Z., Caliskan, H., & Hoang, A. T. (2024). Thermodynamic and exergoenvironmental assessments of solar-assisted combined power cycle using eco-friendly fluids. *Journal of Thermal Analysis and Calorimetry*, *149*(3), 1125-1139.
14. Bai, M., Zhao, L., & Zhao, R. (2022). Review on applications of zeotropic mixtures. *Journal of Thermal Science*, *31*(2), 285-307.
15. Liang, Y., Mckeown, A., Yu, Z., & Alshammari, S. F. K. (2021). Experimental study on a heat driven refrigeration system based on combined organic Rankine and vapour compression cycles. *Energy Conversion and Management*, *234*, 113953.
16. Marion, M., & Louahlia, H. (2021). Volumetric design for ORC-VCC compressor-expander units. *International Journal of Refrigeration*, *132*, 1-10.
17. Bu, X. B., Li, H. S., & Wang, L. B. (2013). Performance analysis and working fluids selection of solar powered organic Rankine-vapor compression ice maker. *Solar energy*, *95*, 271-278.
18. Li, H., Bu, X., Wang, L., Long, Z., & Lian, Y. (2013). Hydrocarbon working fluids for a Rankine cycle powered vapor compression refrigeration system using low-grade thermal energy. *Energy and buildings*, *65*, 167-172.
19. Molés, F., Navarro-Esbrí, J., Peris, B., Mota-Babiloni, A., & Kontomaris, K. K. (2015). Thermodynamic analysis of a combined organic Rankine cycle and vapor compression cycle system activated with low temperature heat sources using low GWP fluids. *Applied Thermal Engineering*, *87*, 444-453.
20. Kim, K. H., & Perez-Blanco, H. (2015). Performance analysis of a combined organic Rankine cycle and vapor compression cycle for power and refrigeration cogeneration. *Applied Thermal Engineering*, *91*, 964-974.

21. Saleh, B. (2016). Parametric and working fluid analysis of a combined organic Rankine-vapor compression refrigeration system activated by low-grade thermal energy. *Journal of advanced research*, *7*(5), 651-660.
22. Nasir, M. T., & Kim, K. C. (2016). Working fluids selection and parametric optimization of an Organic Rankine Cycle coupled Vapor Compression Cycle (ORC-VCC) for air conditioning using low grade heat. *Energy and Buildings*, *129*, 378-395.
23. Marion, M., & Louahlia, H. (2021). Volumetric design for ORC-VCC compressor-expander units. *International Journal of Refrigeration*, *132*, 1-10.
24. Grauberger, A., Young, D., & Bandhauer, T. (2022). Experimental validation of an organic rankine-vapor compression cooling cycle using low GWP refrigerant R1234ze (E). *Applied Energy*, *307*, 118242.
25. Sleiti, A. K., Al-Ammari, W. A., & Al-Khawaja, M. (2023). Experimental investigations on the performance of a thermo-mechanical refrigeration system utilizing ultra-low temperature waste heat sources. *Alexandria Engineering Journal*, *71*, 591-607.
26. Alshammari, S., Kadam, S. T., & Yu, Z. (2023). Assessment of single rotor expander-compressor device in combined organic Rankine cycle (ORC) and vapor compression refrigeration cycle (VCR). *Energy*, *282*, 128763.
27. Witanowski, Ł. (2024). Optimization of an organic rankine cycle–vapor compression cycle system for electricity and cooling production from low-grade waste heat. *Energies*, *17*(22), 5566.
28. Suchocki, T. (2025). Introduction to ORC–VCC systems: a review. Energies, 18(1), 171.
29. Popov, V. L. (2017). Coulomb's law of friction. In *Contact mechanics and friction: physical principles and applications* (pp. 151-172). Berlin, Heidelberg: Springer Berlin Heidelberg.
30. Bell, I. H., Wronski, J., Quoilin, S., & Lemort, V. (2014). Pure and pseudo-pure fluid thermophysical property evaluation and the open-source thermophysical property library CoolProp. *Industrial & engineering chemistry research*, *53*(6), 2498.
31. Gongnan, X. I. E., Xiaoxiao, X. U., Xianliang, L. E. I., Zhouhang, L. I., & Yong, L. I. (2022). Heat transfer behaviors of some supercritical fluids: A review. *Chinese Journal of Aeronautics*, *35*(1), 290-306.
32. Liang, Y., Sun, Z., Dong, M., Lu, J., & Yu, Z. (2020). Investigation of a refrigeration system based on combined supercritical CO2 power and transcritical CO2 refrigeration cycles by waste heat recovery of engine. *International Journal of Refrigeration*, *118*, 470-482.
33. Yu, A., Su, W., Lin, X., Zhou, N., & Zhao, L. (2020). Thermodynamic analysis on the combination of supercritical carbon dioxide power cycle and transcritical carbon dioxide refrigeration cycle for the waste heat recovery of shipboard. *Energy conversion and management*, *221*, 113214.